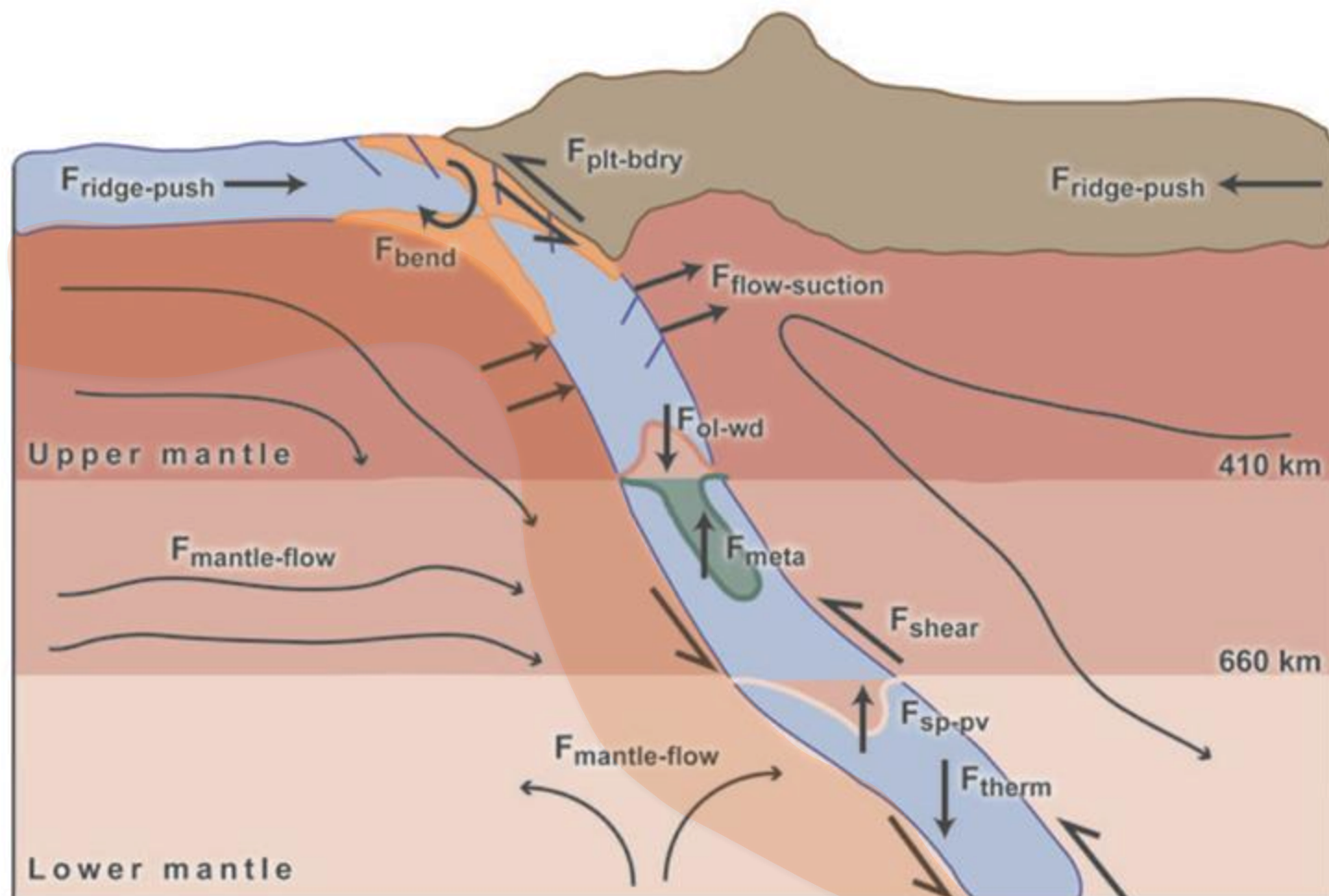
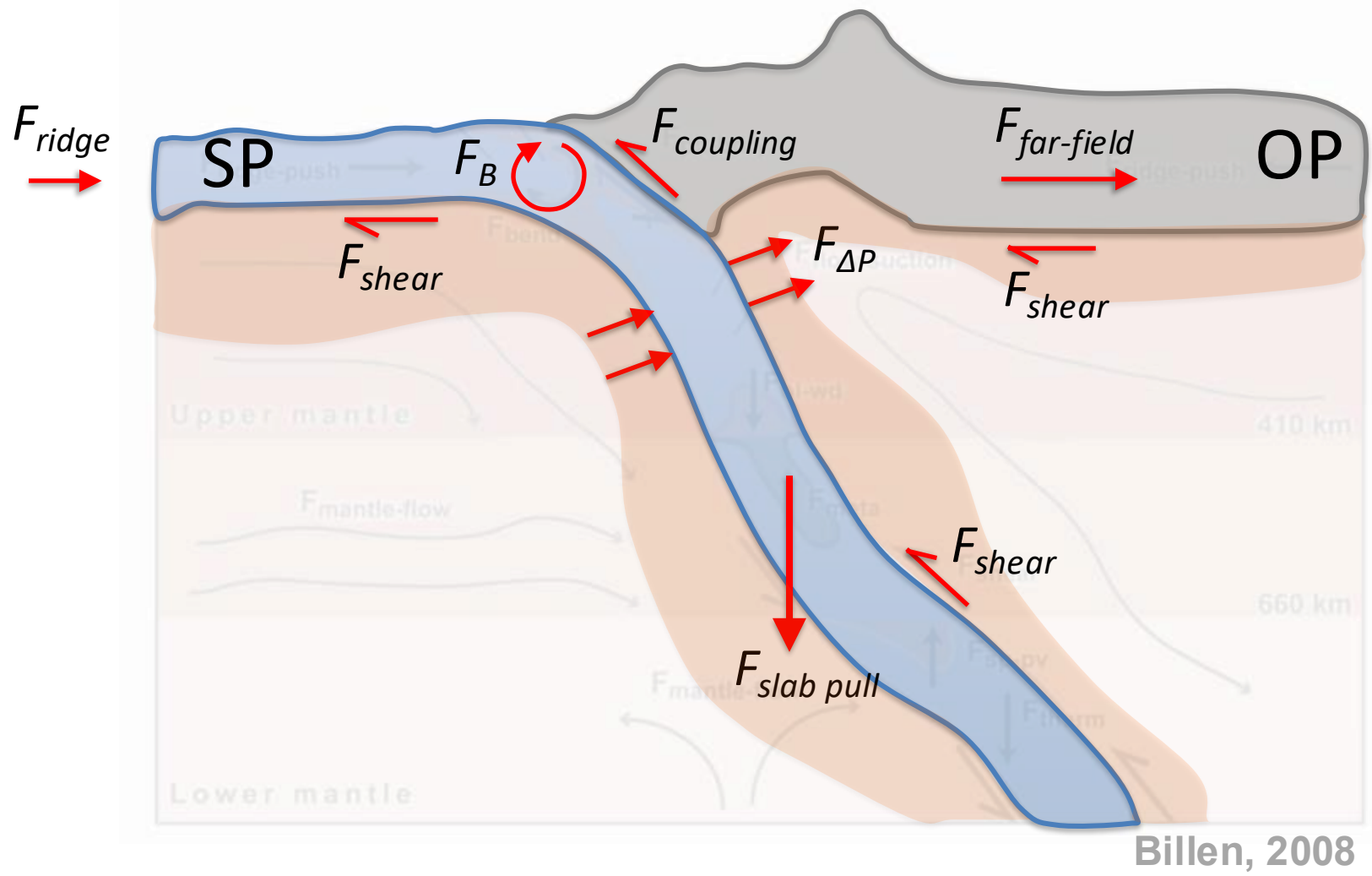
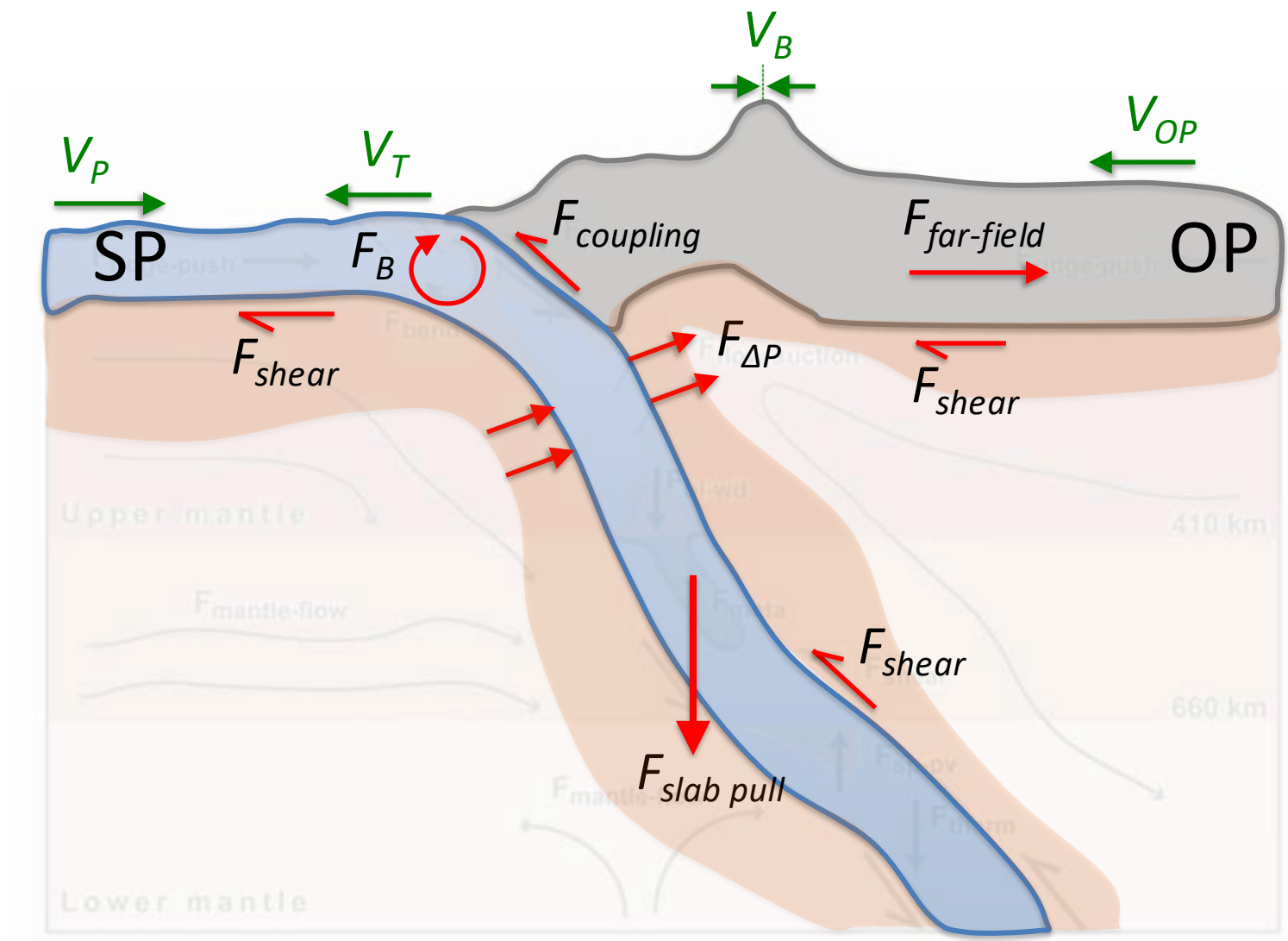


Mantle rheology and subduction dynamics



Billen, 2008



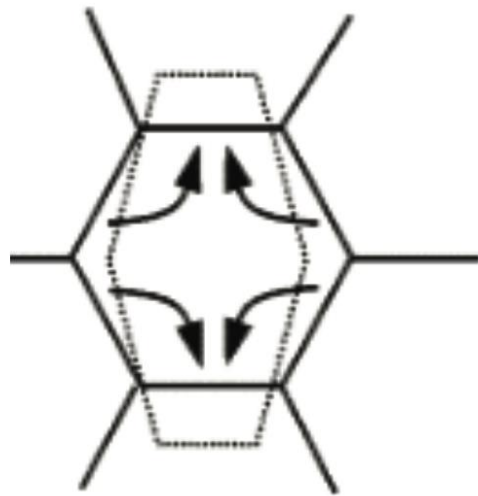


FORCES

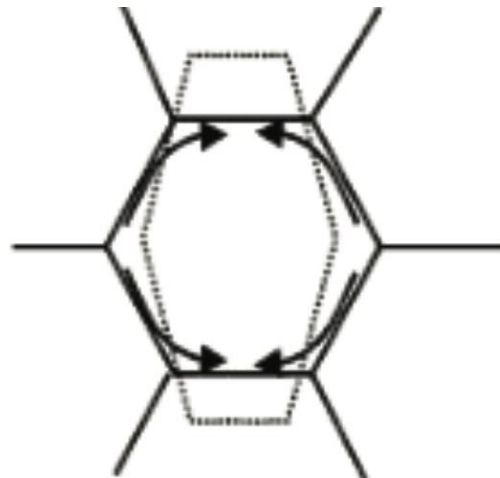
OBSERVABLE KINEMATICS

Diffusion creep

Nabarro-Herring creep



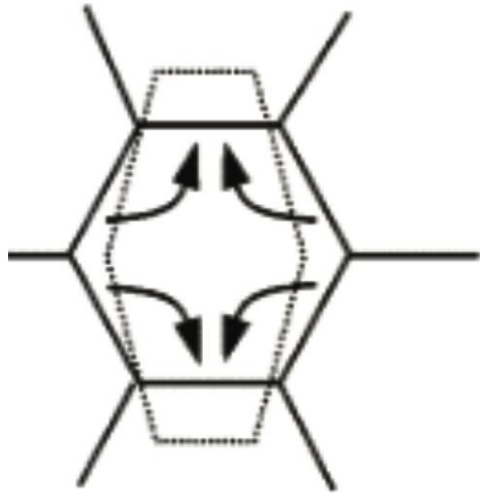
Coble creep



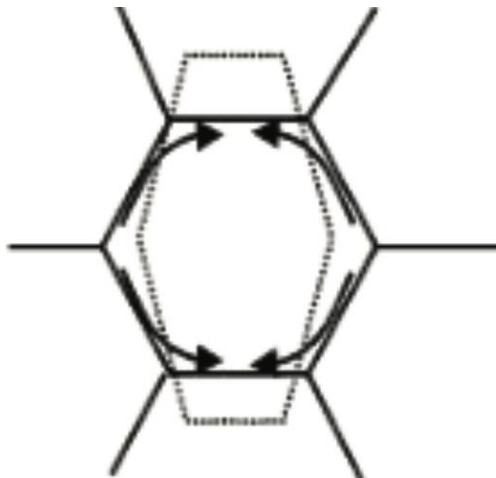
- *Diffusion of atoms through the interiors and along boundaries of crystal grains when the grains are subjected to stress.*
- *As a result of this, the grains deform leading to strain.*
- *Produces Newtonian fluid behavior.*

Diffusion Dislocation creep

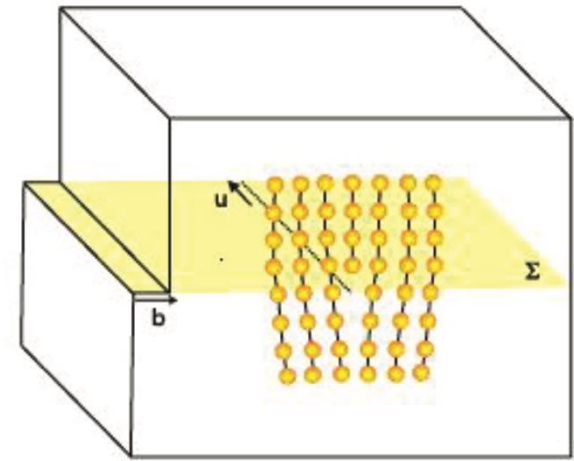
Nabarro-Herring creep



Coble creep



Dislocation creep



- *The other endmember of high- T , high- P fluid deformation of mantle material.*
- *Deformation occurs via the migration of dislocations (linear imperfections in the crystal lattice structure).*
- *Produces non-Newtonian (power-law) fluid behavior*

Figuring out the parameters...

Experiments:

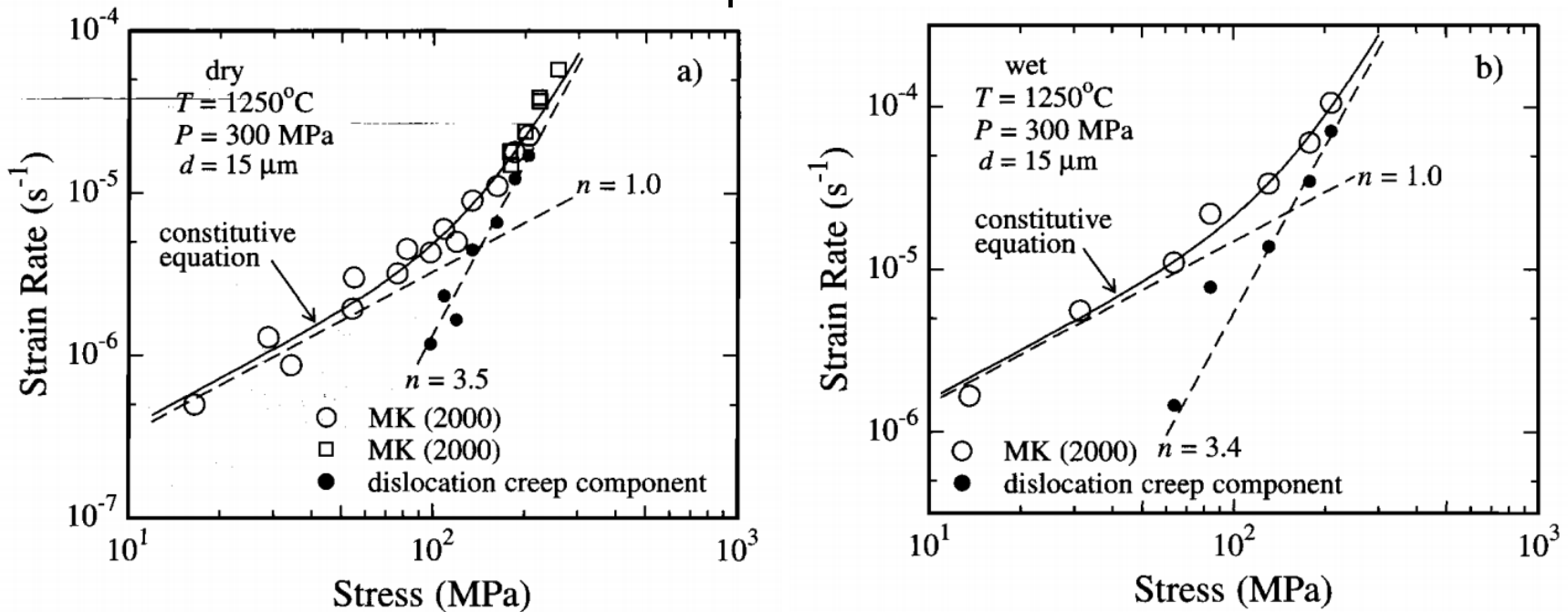


Figure 2. Plots of strain rate versus differential stress for fine-grained olivine aggregates deformed under dry (a) and wet (b) conditions. For both data sets, a transition from diffusion creep to dislocation creep occurs with an increase in differential stress. Non-linear fits to the data using equation 2 (labeled constitutive equation) and linear fits to the high stress dislocation creep component of the total strain rate are shown in both figures. These data are from the studies of *Mei and Kohlstedt* [2000a, 2000b].

Dislocation and diffusion creep

Result: A generic flow law to describe olivine diffusion and dislocation creep:

$$\dot{\varepsilon} = A\sigma^n d^{-p} f_{H_20}^r \exp(\alpha\phi) \exp\left[-\frac{E + PV}{RT}\right]$$

Dislocation and diffusion creep

Result: A generic flow law to describe olivine diffusion and dislocation creep:

$$\dot{\varepsilon} = A\sigma^n d^{-p} f_{H_20}^r \exp(\alpha\phi) \exp\left[-\frac{E + PV}{RT}\right]$$

Table 1: Rheological Parameters for Equation (1).

| | A^a | n | p | r^b | α | E^* (kJ/mol) | V^* (10^{-6} m 3 /mol) |
|--|--------------------------------|---------------|-----|---------------|----------|-------------------|-----------------------------------|
| dry diffusion | 1.5×10^9 | 1 | 3 | - | 30 | 375 ± 50 | 2-10 |
| wet diffusion | 2.5×10^7 ^d | 1 | 3 | 0.7-1.0 | 30 | 375 ± 75 | 0-20 |
| wet diffusion (constant C _{OH}) ^c | 1.0×10^6 | 1 | 3 | 1 | 30 | 335 ± 75 | 4 |
| dry dislocation | 1.1×10^5 | 3.5 ± 0.3 | 0 | - | 30-45 | 530 ± 4 | (see Table 2) |
| wet dislocation | 1600 | 3.5 ± 0.3 | 0 | 1.2 ± 0.4 | 30-45 | 520 ± 40 | 22 ± 11 |
| wet dislocation (constant C _{OH}) ^e | 90 | 3.5 ± 0.3 | 0 | 1.2 | 30-45 | 480 ± 40 | 11 |
| dry GBS, T>1250°C | 4.7×10^{10} | 3.5 | 2 | - | 30-45 | 600^f | (see Table 2) ^g |
| dry GBS, T<1250°C | 6500 | 3.5 | 2 | - | 30-45 | 400^f | (see Table 2) ^g |

Dislocation and diffusion creep

Result: A generic flow law to describe olivine diffusion and dislocation creep:

$$\dot{\varepsilon} = A\sigma^n d^{-p} f_{H_20}^r \exp(\alpha\phi) \exp\left[-\frac{E + PV}{RT}\right]$$

Table 1: Rheological Parameters for Equation (1).

| | A^a | n | p | r^b | α | E^* (kJ/mol) | V^* (10^{-6} m 3 /mol) |
|--|--------------------------------|---------------|-----|---------------|----------|-------------------|-----------------------------------|
| dry diffusion | 1.5×10^9 | 1 | 3 | - | 30 | 375 ± 50 | 2-10 |
| wet diffusion | 2.5×10^7 ^d | 1 | 3 | 0.7-1.0 | 30 | 375 ± 75 | 0-20 |
| wet diffusion (constant C _{OH}) ^c | 1.0×10^6 | 1 | 3 | 1 | 30 | 335 ± 75 | 4 |
| dry dislocation | 1.1×10^5 | 3.5 ± 0.3 | 0 | - | 30-45 | 530 ± 4 | (see Table 2) |
| wet dislocation | 1600 | 3.5 ± 0.3 | 0 | 1.2 ± 0.4 | 30-45 | 520 ± 40 | 22 ± 11 |
| wet dislocation (constant C _{OH}) ^e | 90 | 3.5 ± 0.3 | 0 | 1.2 | 30-45 | 480 ± 40 | 11 |
| dry GBS, T>1250°C | 4.7×10^{10} | 3.5 | 2 | - | 30-45 | 600 ^f | (see Table 2) ^g |
| dry GBS, T<1250°C | 6500 | 3.5 | 2 | - | 30-45 | 400 ^f | (see Table 2) ^g |

Note:

- $n = 1$ for **diffusion creep** (Newtonian), $n \approx 3.5$ for **dislocation creep**.
- No grain size dependence for **dislocation creep** ($p = 0$)

Dislocation and diffusion creep

Result: A generic flow law to describe olivine diffusion and dislocation creep:

$$\dot{\varepsilon} = A\sigma^n d^{-p} f_{H_20}^r \exp(\alpha\phi) \exp\left[-\frac{E + PV}{RT}\right]$$

Following $\sigma = 2\mu\dot{\varepsilon}_{xx}$, can also re-arrange to get an effective viscosity

$$\mu_{diff/disl} = \left(\frac{d^p}{A f_{H20}^r}\right)^{\frac{1}{n}} \dot{\varepsilon}^{\frac{1-n}{n}} \exp\left[\frac{E + PV}{nRT}\right]$$

Note:
melt now neglected

Dislocation and diffusion creep

Result: A generic flow law to describe olivine diffusion and dislocation creep:

$$\dot{\varepsilon} = A\sigma^n d^{-p} f_{H_20}^r \exp(\alpha\phi) \exp\left[-\frac{E + PV}{RT}\right]$$

Following $\sigma = 2\mu\dot{\varepsilon}_{xx}$, can also re-arrange to get an effective viscosity

$$\mu_{diff/disl} = \left(\frac{d^p}{A f_{H20}^r}\right)^{\frac{1}{n}} \dot{\varepsilon}^{\frac{1-n}{n}} \exp\left[\frac{E + PV}{nRT}\right]$$

Note:
melt now neglected

Both deformation mechanisms will typically be active at the same time.

$$\dot{\varepsilon} = \dot{\varepsilon}_{disl} + \dot{\varepsilon}_{diff} = A_{disl}\sigma^n + A_{diff}\sigma d^3$$

(This common microphysical assumption leads to dominance of the weakest deformation mechanism.)

Dislocation and diffusion creep

Result: A generic flow law to describe olivine diffusion and dislocation creep:

$$\dot{\varepsilon} = A\sigma^n d^{-p} f_{H_20}^r \exp(\alpha\phi) \exp\left[-\frac{E + PV}{RT}\right]$$

Following $\sigma = 2\mu\dot{\varepsilon}_{xx}$, can also re-arrange to get an effective viscosity

$$\mu_{diff/disl} = \left(\frac{d^p}{A f_{H20}^r}\right)^{\frac{1}{n}} \dot{\varepsilon}^{\frac{1-n}{n}} \exp\left[\frac{E + PV}{nRT}\right]$$

Note:
melt now neglected

Both deformation mechanisms will typically be active at the same time.

$$\dot{\varepsilon} = \dot{\varepsilon}_{disl} + \dot{\varepsilon}_{diff} = A_{disl}\sigma^n + A_{diff}\sigma d^3$$

$$\frac{1}{\mu_{eff}} = \frac{1}{\mu_{diff}} + \frac{1}{\mu_{disl}}$$

μ_{comp} = composite
viscosity (dominated by
weakest phase!)

Dislocation and diffusion creep and ...

Result: A generic flow law to describe olivine diffusion and dislocation creep:

$$\dot{\varepsilon} = A\sigma^n d^{-p} f_{H_20}^r \exp(\alpha\phi) \exp\left[-\frac{E + PV}{RT}\right]$$

Following $\sigma = 2\mu\dot{\varepsilon}_{xx}$, can also re-arrange to get an effective viscosity

$$\mu_{diff/disl} = \left(\frac{d^p}{A f_{H20}^r}\right)^{\frac{1}{n}} \dot{\varepsilon}^{\frac{1-n}{n}} \exp\left[\frac{E + PV}{nRT}\right]$$

Note:
melt now neglected

Both deformation mechanisms will typically be active at the same time.

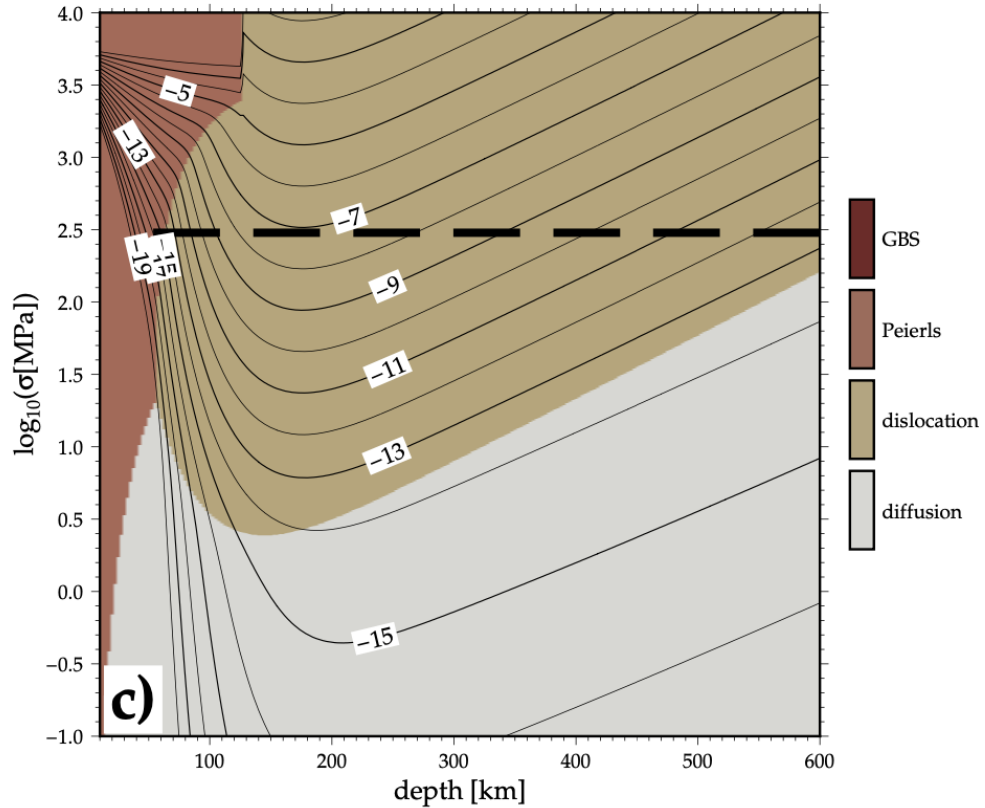
$$\dot{\varepsilon} = \dot{\varepsilon}_{disl} + \dot{\varepsilon}_{diff} = A_{disl}\sigma^n + A_{diff}\sigma d^{-3}$$

$$\frac{1}{\mu_{eff}} = \frac{1}{\mu_{diff}} + \frac{1}{\mu_{disl}} + \frac{1}{\mu_{Peierls}}$$

And can consider other
deformation styles (e.g.,
low-T plasticity)

Dislocation and diffusion creep and ...

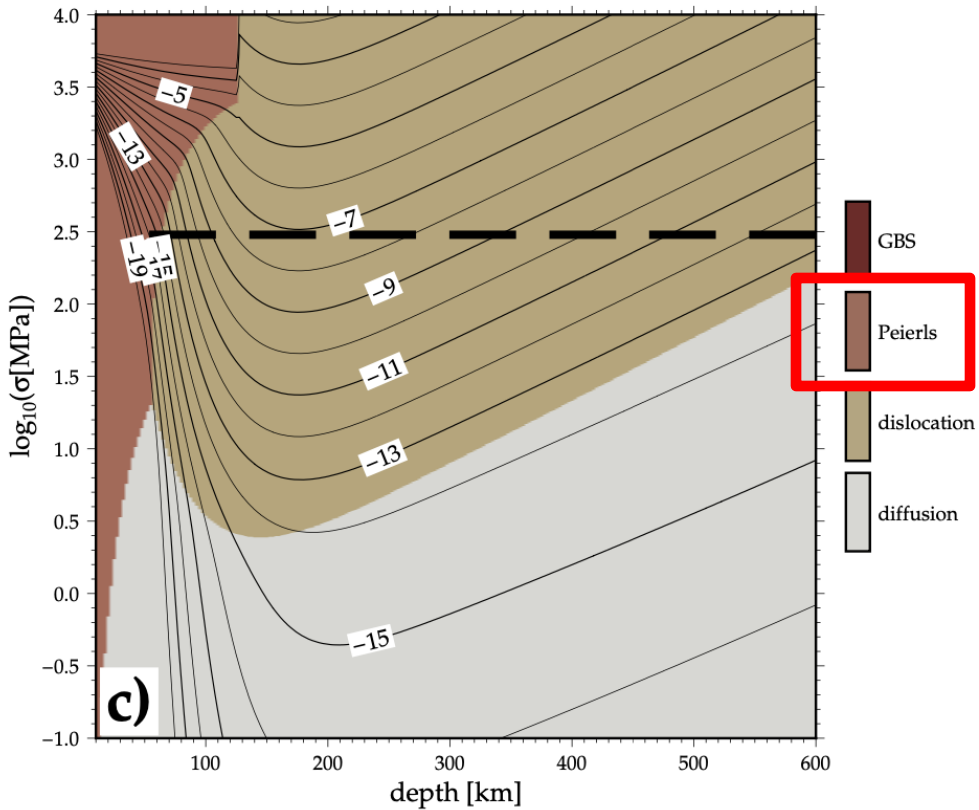
A deformation map for olivine
under dry conditions



Becker and Faccenna

Dislocation and diffusion creep and ...

A deformation map for olivine under dry conditions



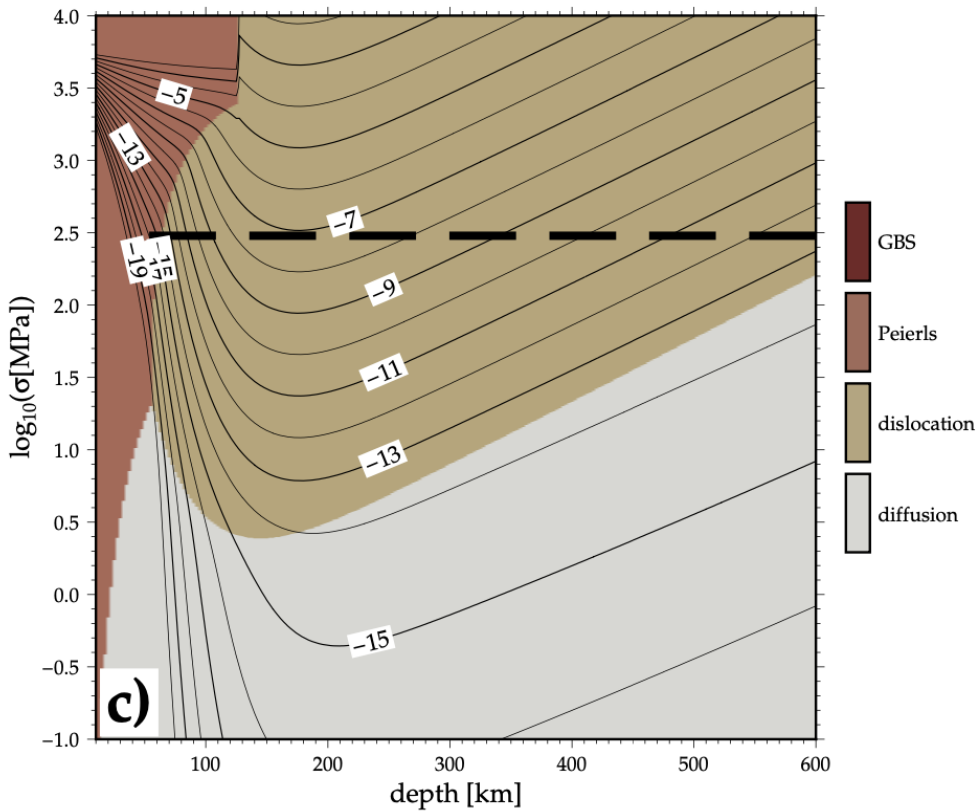
Peierls mechanism/creep:

- Strain rates increase more rapidly than power-law predicts.
- This occurs as stresses approach the *Peierls stress*.
- Physically: the stress needed to move a dislocation without the help of thermal activation.
- See, e.g., Karato (2008) book for mechanistic explanation.

Becker and Faccenna

Dislocation and diffusion creep and ...

A deformation map for olivine under dry conditions

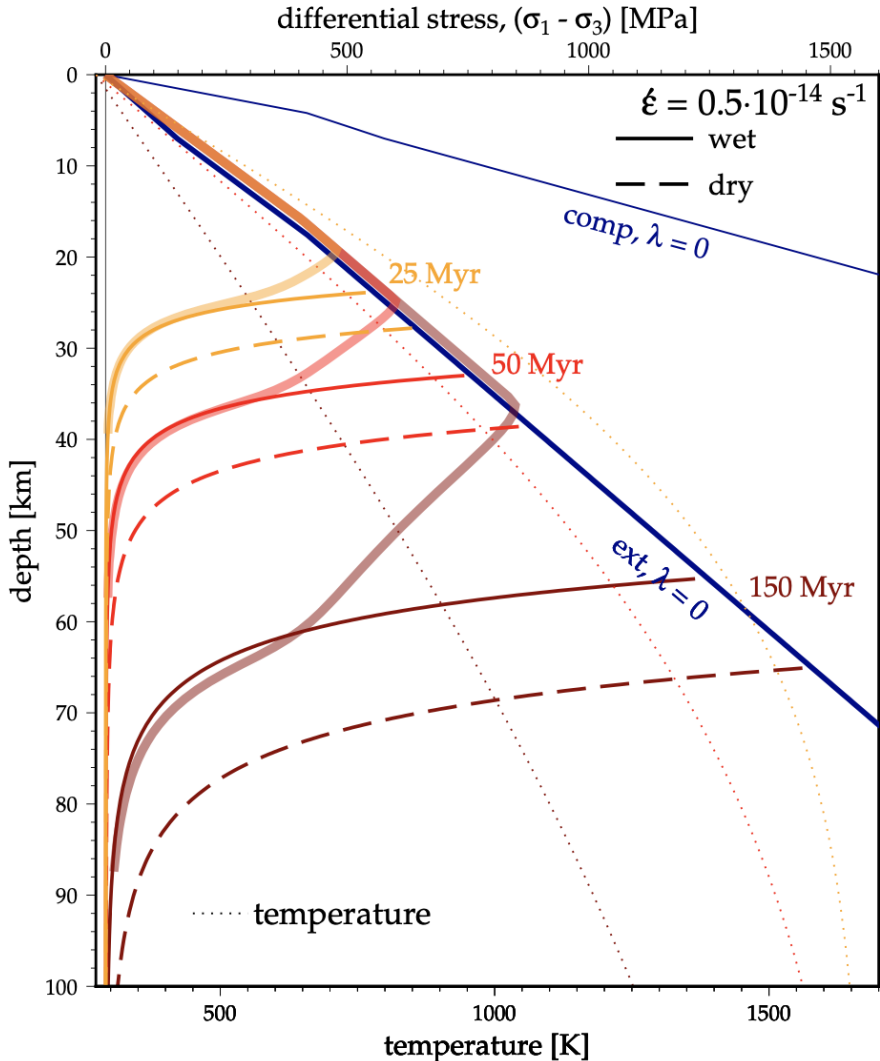


Becker and Faccenna

How deep does dislocation creep operate in the mantle?

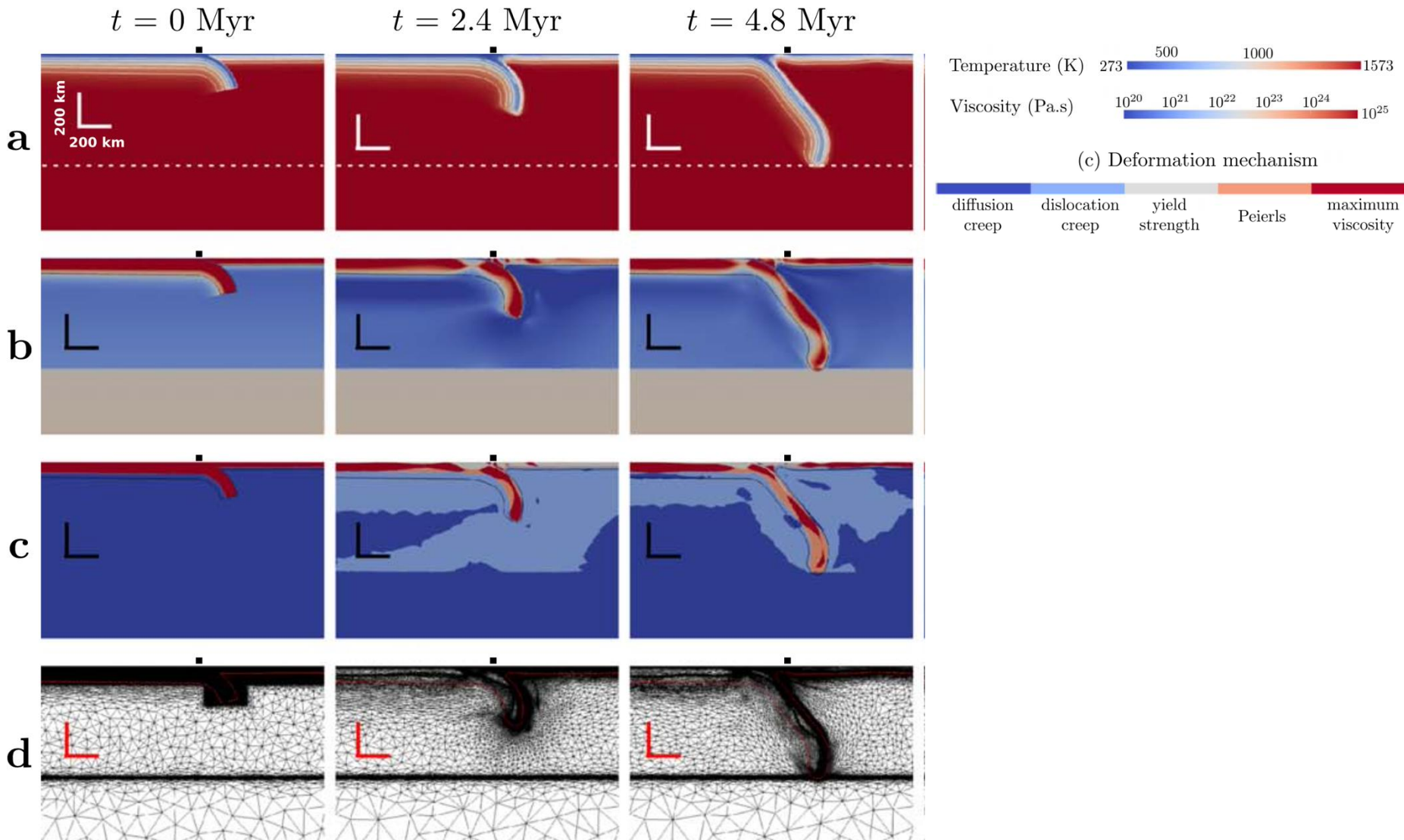
- Mantle convection strain rates between $\sim 10^{-15}$ and 10^{-12} s^{-1} .
- From, indicates dislocation creep regime in a range of depths below the lithosphere from $\sim 100\text{-}300 \text{ km}$, at deviatoric stresses of $\sim 10 \text{ MPa}$ (cf. Podolefsky et al., 2004; Becker, 2006; Behn et al., 2009).
- While grain sizes are uncertain and evolving, this also means that the $\sim \text{mm}$ grain sizes provide an explanation for why CPOs from dislocation creep may be concentrated at those asthenospheric depths

Deformation in the lithosphere



- Today's discussion: Flow laws. For depths > brittle-to-ductile transition
- Above which, brittle and elastic rheologies dominate (i.e., are weaker and so dominate strain/strain rate).
- Here's a strength profile (constant strain rate) for temperatures associated with a cooling oceanic plate.
- For top-to-bottom: Brittle, Peierl's creep, and dislocation creep rheologies.

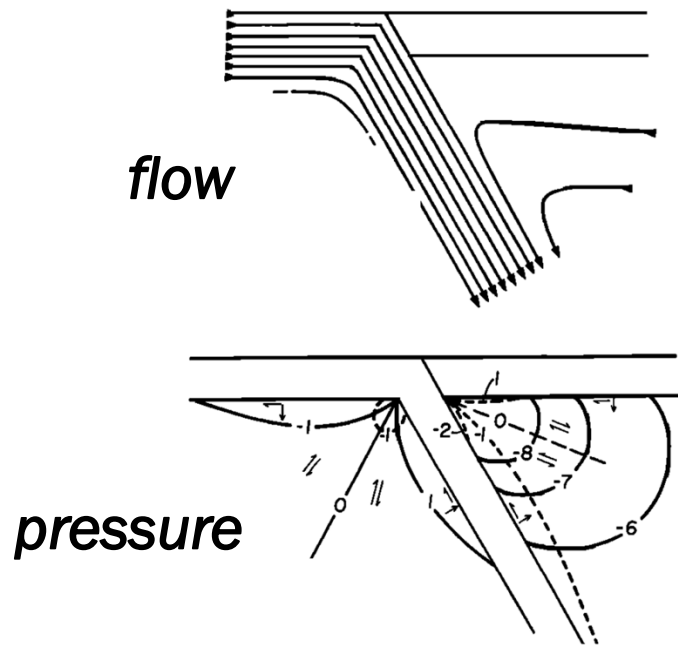
When we plug these flow laws into subduction models...



(non-slab) Mantle rheology and subduction dynamics

(non-slab) Mantle rheology and subduction dynamics

Dislocation creep (power-law) flow in the mantle wedge affects corner flow and the associated dynamic pressure:



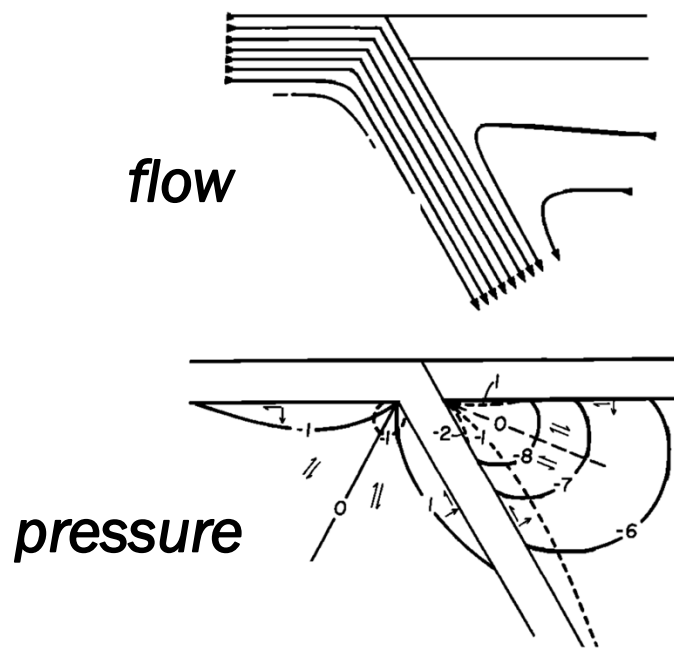
Tovish et al., 1978

cf. McKenzie, 1969; Stevenson and Turner, 1977

Lower magnitude mantle
wedge P

(non-slab) Mantle rheology and subduction dynamics

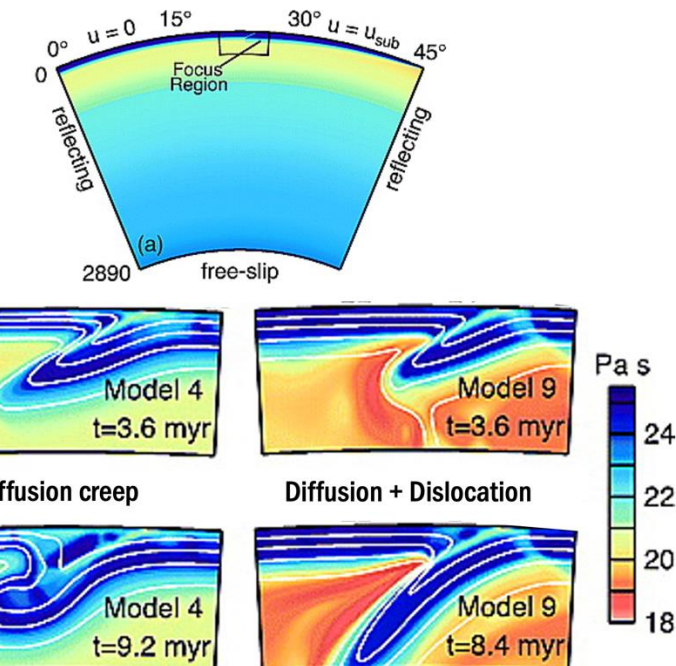
Dislocation creep (power-law) flow in the mantle wedge affects corner flow and the associated dynamic pressure:



Tovish et al., 1978

cf. McKenzie, 1969; Stevenson and Turner, 1977

Lower magnitude mantle
wedge P



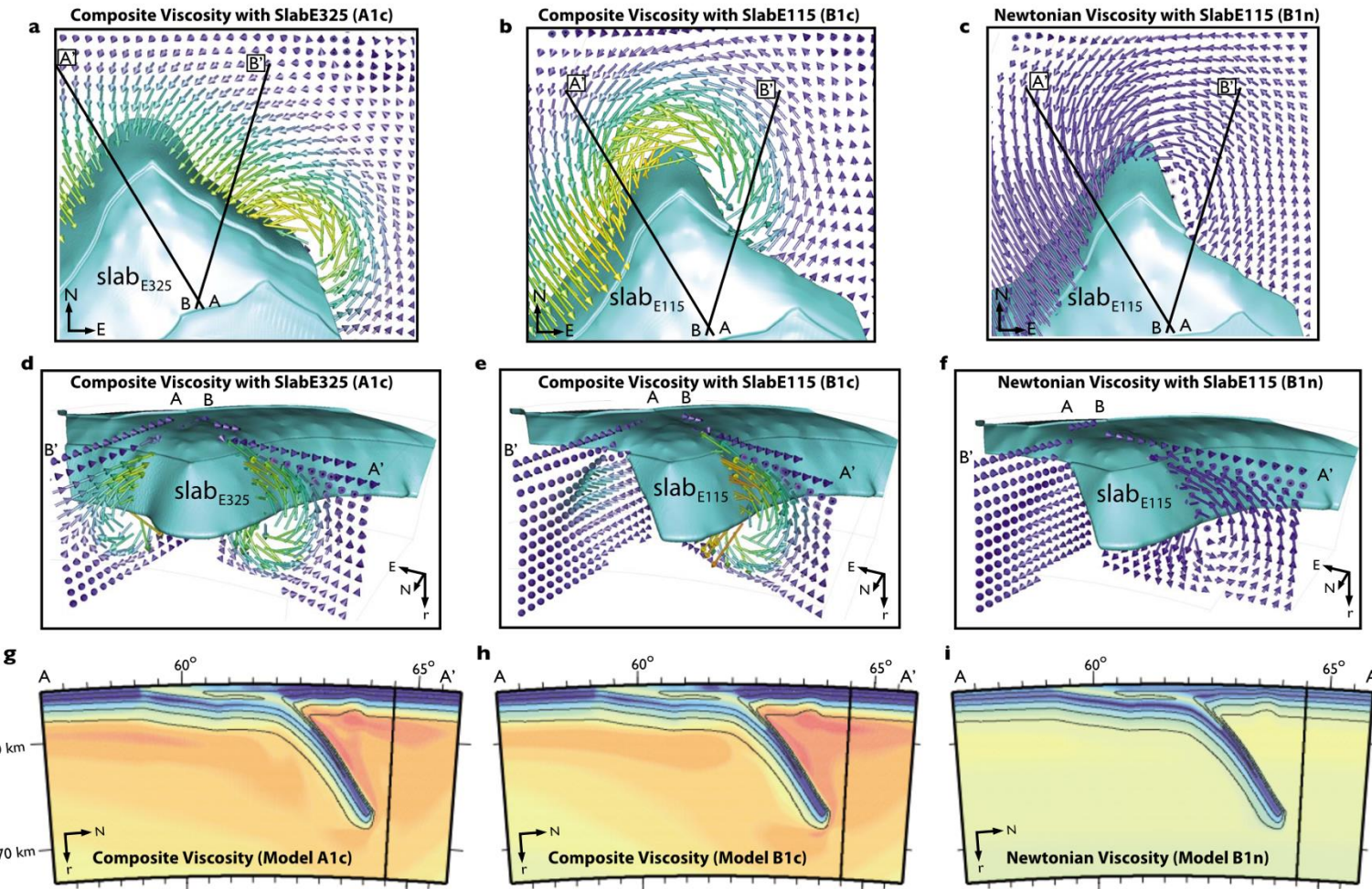
Billen and Hirth, 2005

Cf. Billen and Hirth, 2007

So, steeper dips

(non-slab) Mantle rheology and subduction dynamics

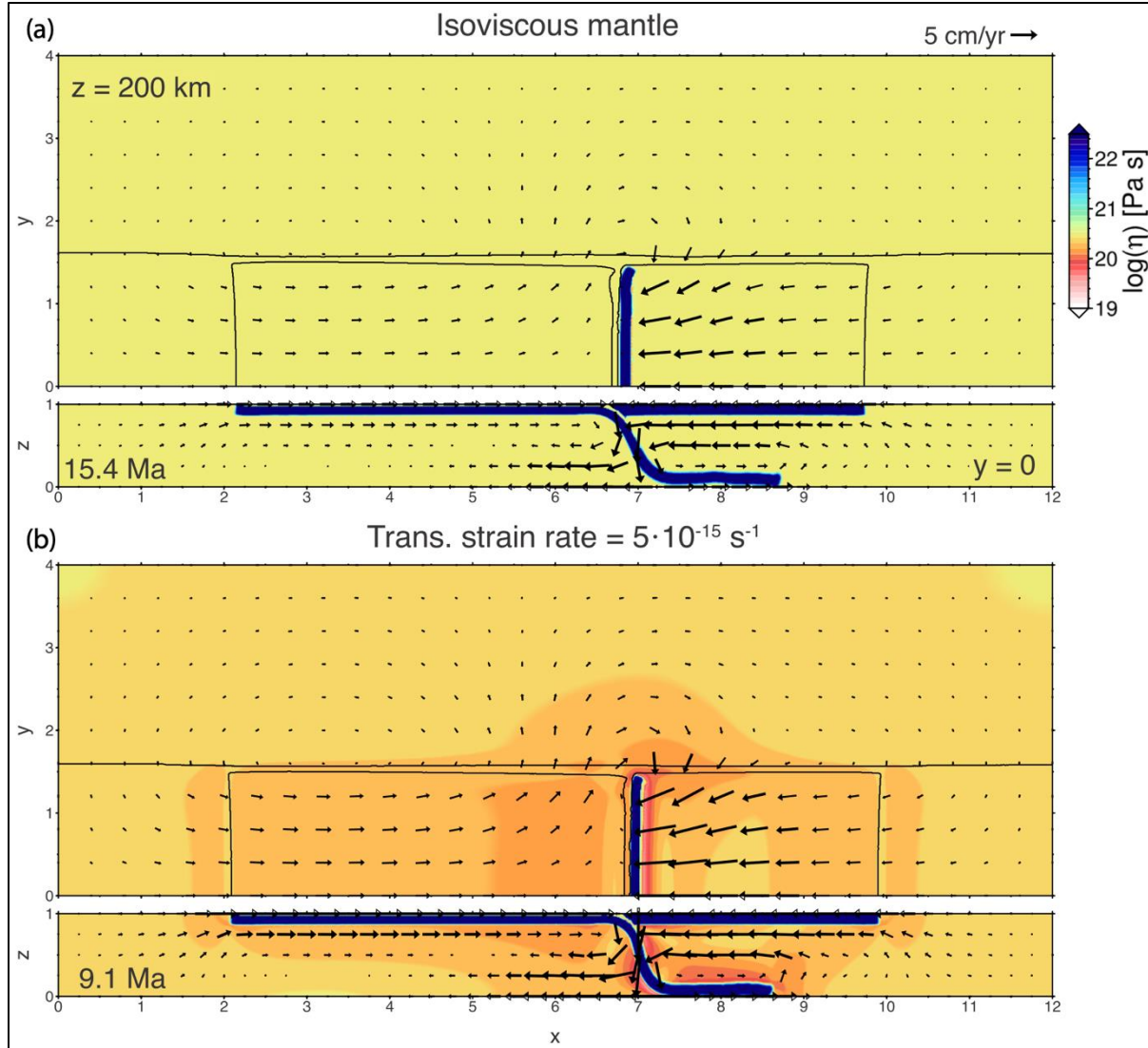
Power-law flow and 3-D mantle flow regime



Jadamec & Billen (2010; 2012): Rapid mantle flow around a slab edge in Alaska

(non-slab) Mantle rheology and subduction dynamics

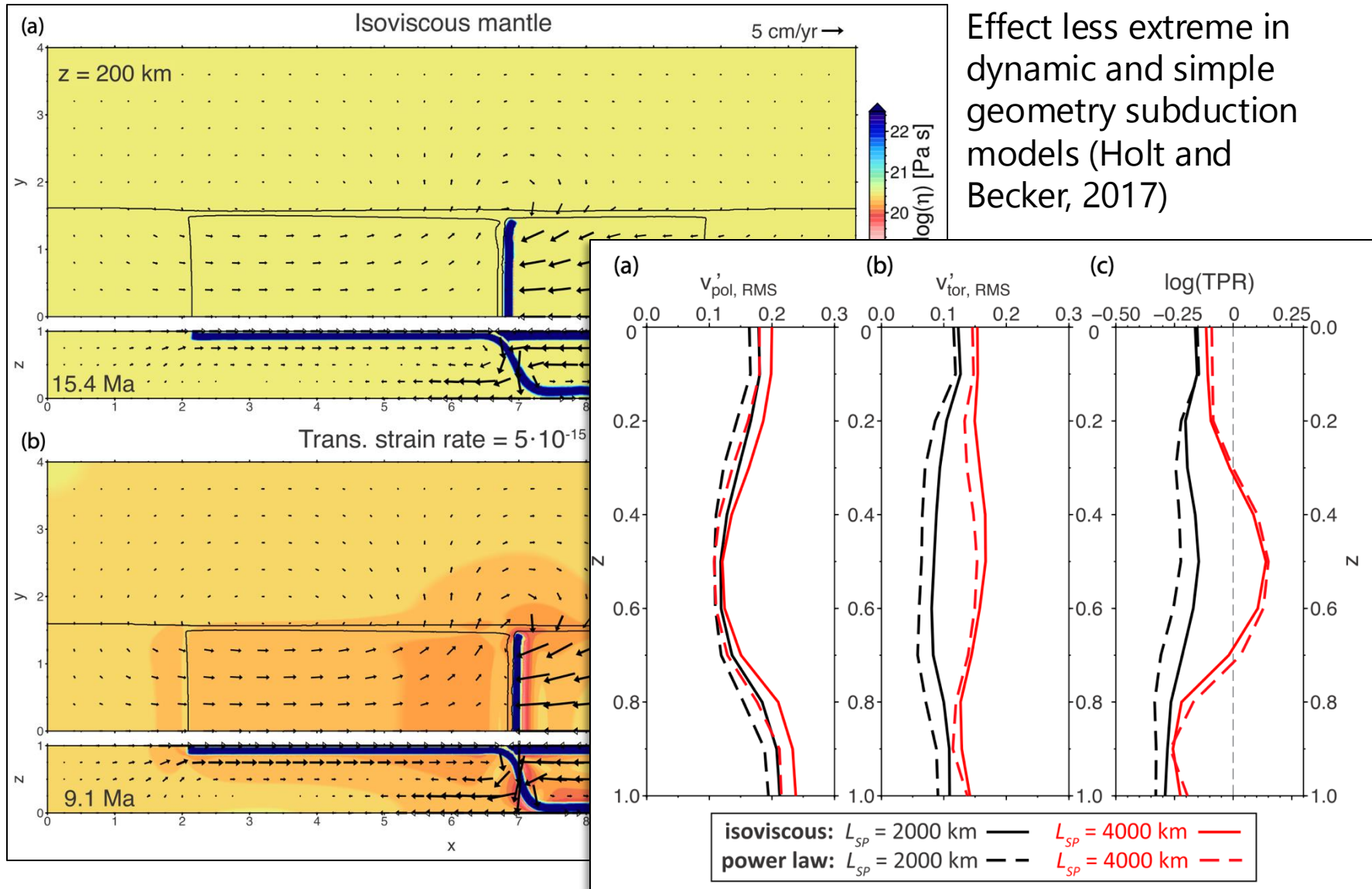
Power-law flow and 3-D mantle flow regime



Effect less extreme in dynamic and simple geometry subduction models (Holt and Becker, 2017)

(non-slab) Mantle rheology and subduction dynamics

Power-law flow and 3-D mantle flow regime



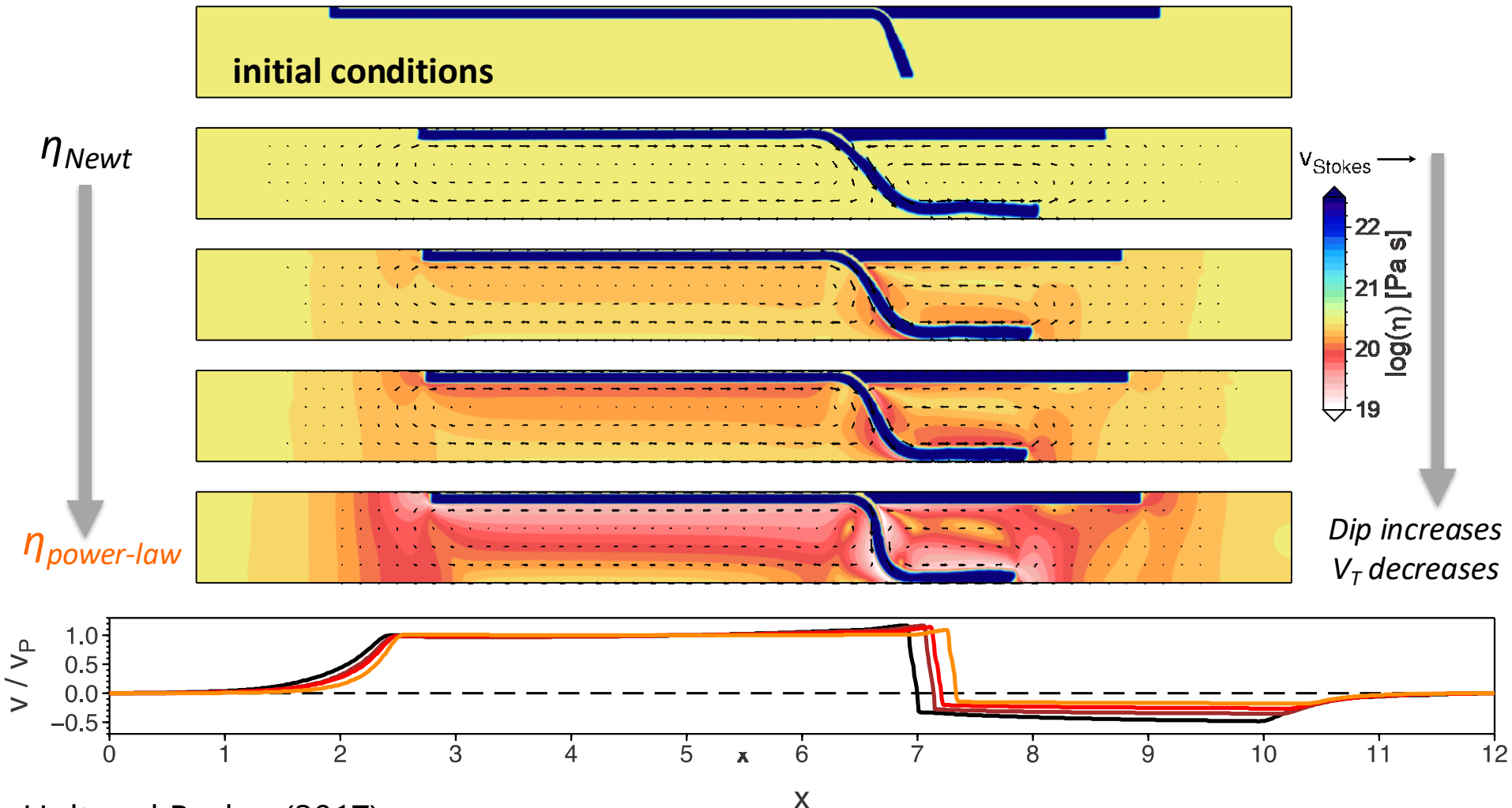
(non-slab) Mantle rheology and subduction dynamics

Power-law flow and plate and trench motions

(non-slab) Mantle rheology and subduction dynamics

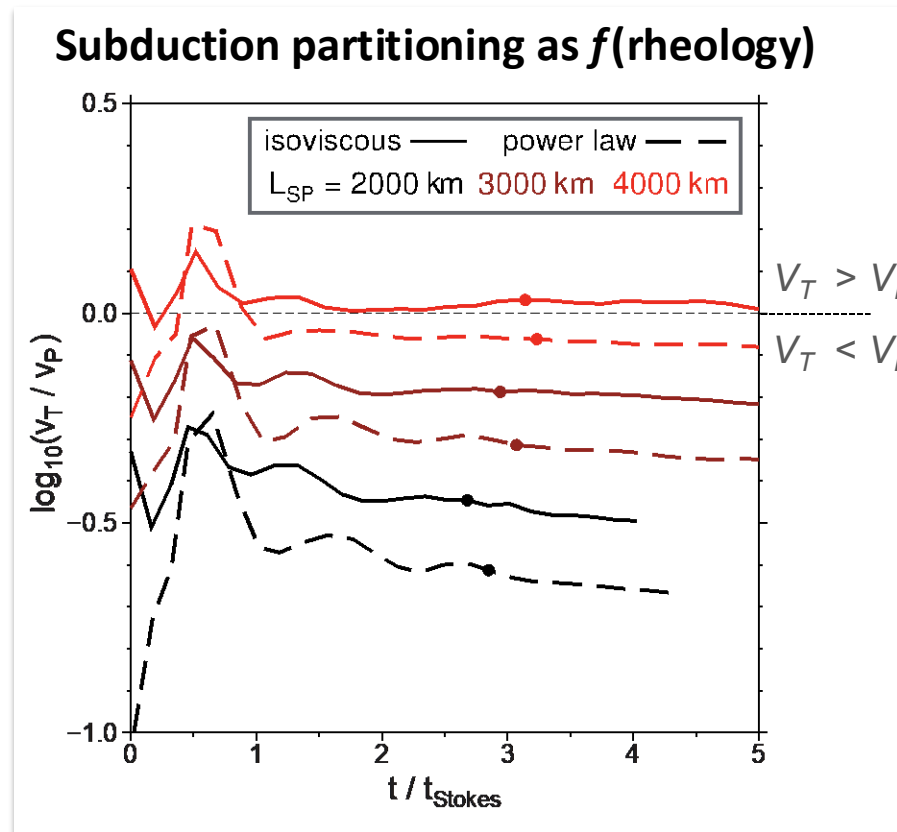
Power-law flow and plate and trench motions

Two-dimensional models (Wide trench!)



(non-slab) Mantle rheology and subduction dynamics

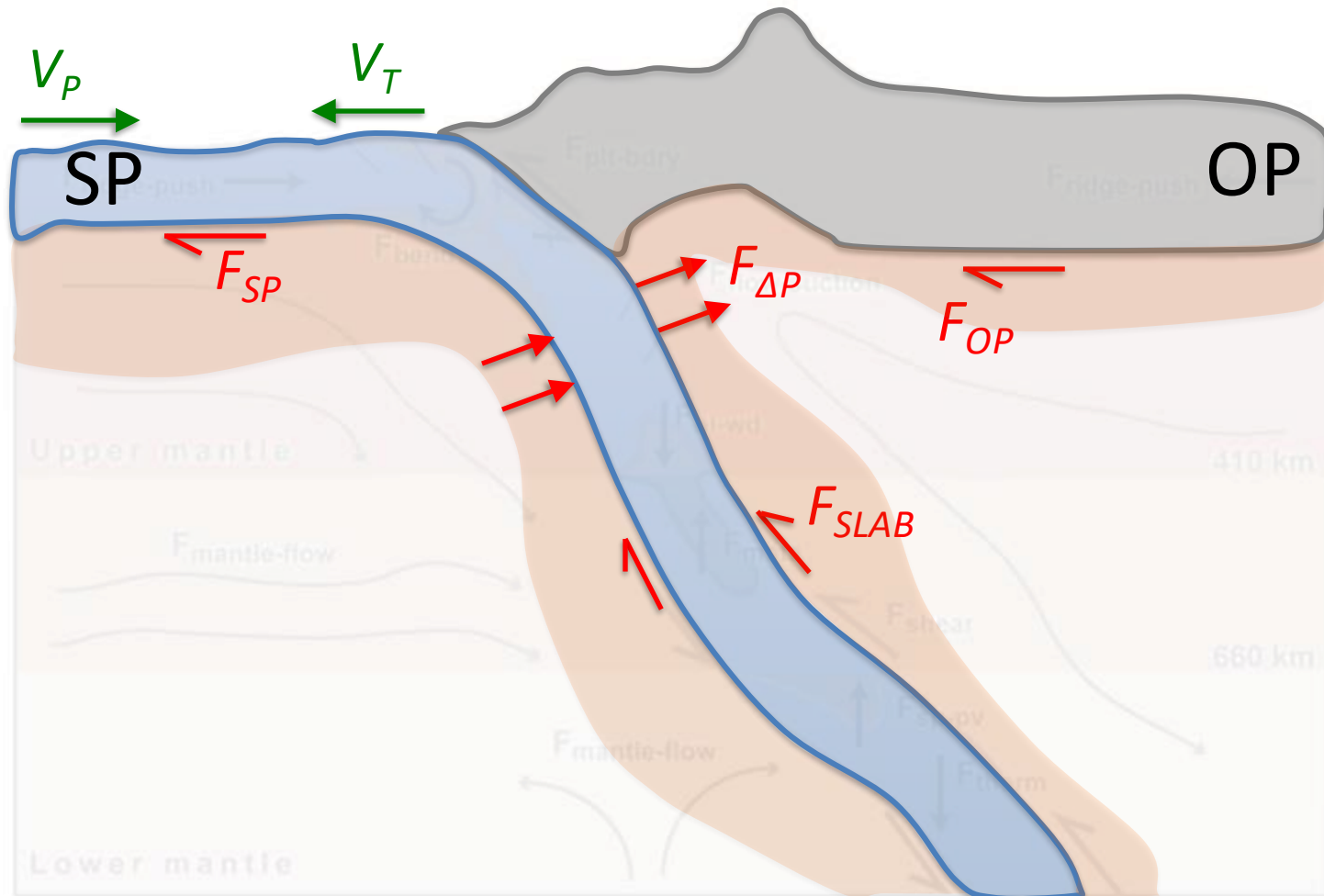
Power-law flow and plate and trench motions



- Power-law mantle rheology reduces rates of relative trench retreat, V_T / V_P
- To understand why, we estimate magnitude of relevant forces (i.e., forces associated with mantle flow).

(non-slab) Mantle rheology and subduction dynamics

Power-law flow and plate and trench motions



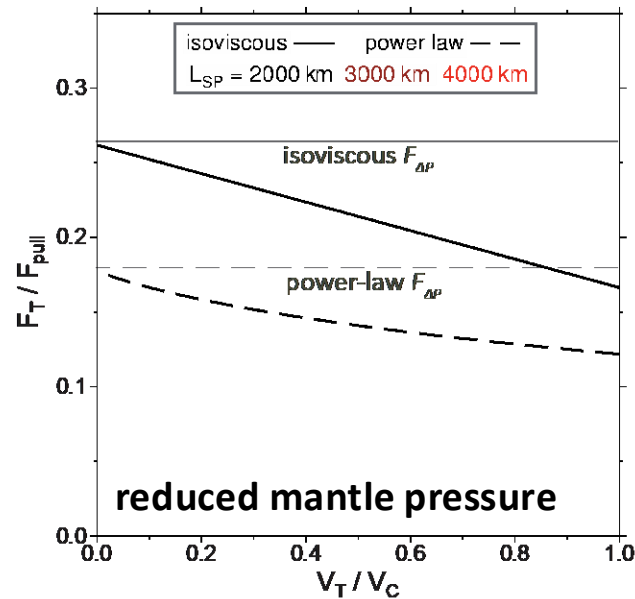
$$\text{Forces resisting } V_P = 2F_{SLAB} + F_{SP} + F_{OP}$$

$$\text{Forces resisting } V_T = F_{\Delta P} - F_{OP}$$

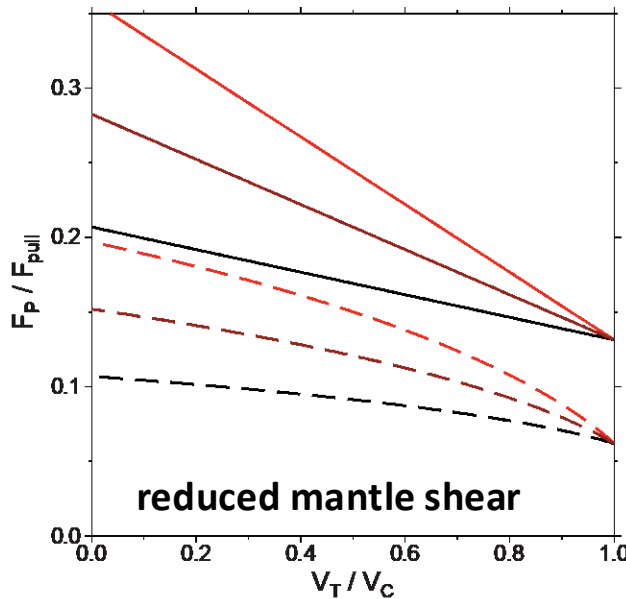
(non-slab) Mantle rheology and subduction dynamics

Power-law flow and plate and trench motions

Force resisting V_T



Force resisting V_P

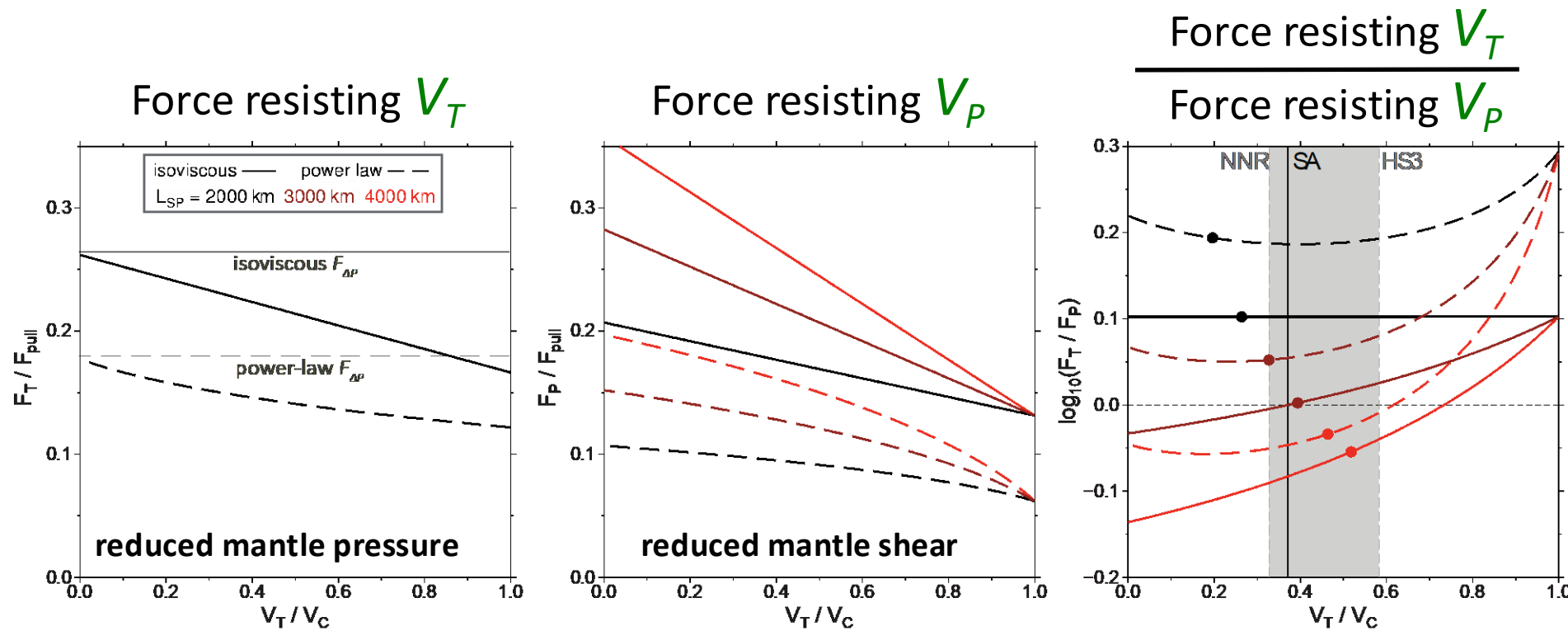


Forces resisting V_P = $2F_{SLAB} + F_{SP}$: Reduced by power law mantle (i.e., shear adjacent to plates)

Forces resisting V_T = $F_{\Delta P} - F_{OP}$: Reduced by power law mantle (e.g. Tovich et al., 1978).

(non-slab) Mantle rheology and subduction dynamics

Power-law flow and plate and trench motions



Forces resisting V_P = $2F_{SLAB} + F_{SP}$: Reduced by power law mantle (i.e., shear adjacent to plates)

Forces resisting V_T = $F_{\Delta P} - F_{OP}$: Reduced by power law mantle (e.g. Tovich et al., 1978).

Force resisting V_T

Force resisting V_P : Increased by power law mantle

(non-slab) Mantle rheology and subduction dynamics

Power-law flow and plate and trench motions

Geophysical Research Letters

RESEARCH LETTER

10.1029/2019GL085212

Key Points:

- Numerical models show that a very weak and thin upper asthenosphere layer can alone reduce trench retreat and enhance plate motion
- The impact of this effect depends on the relative contrast between the effective stiffness of the lithosphere and the underlying mantle
- This regional mechanism explains the high convergence and low trench migration rates observed globally at natural subduction zones

Supporting Information:

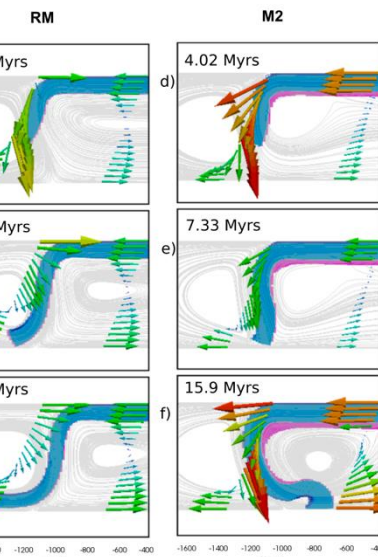
- Supporting Information S1

The Impact of a Very Weak and Thin Upper Asthenosphere on Subduction Motions

R. Carluccio^{1,2,3} , B. Kaus² , F. A. Capitanio⁴ , and L. N. Moresi^{1,5} 

¹School of Earth Sciences, University of Melbourne, Melbourne, Victoria, Australia, ²Institute of Geosciences, Johannes Gutenberg University Mainz, Mainz, Germany, ³Department of Geosciences, University of Padua, Padua, Italy, ⁴School of Earth, Atmosphere and Environment, Monash University, Clayton, Victoria, Australia, ⁵Research School of Earth Sciences, Australian National University, Canberra, ACT, Australia

Abstract Recent geophysical observations report the presence of a very weak and thin upper asthenosphere underneath subducting oceanic plates at convergent margins. Along these margins, trench migrations are significantly slower than plate convergence rates. We use numerical models to assess the role of a weak upper asthenospheric layer on plate and trench motions. We show that the presence of this layer alone can enhance an advancing trend for the motion of the plate and hamper trench retreat. This mechanism provides a novel and alternative explanation for the slow rates of trench migration and fast-moving plates observed globally at natural subduction zones.



JGR Solid Earth

Research Article

The Effect of a Weak Asthenospheric Layer on Surface Kinematics, Subduction Dynamics and Slab Morphology in the Lower Mantle

Nestor G. Cerpa , Karin Sigloch, Fanny Garel, Arnauld Heuret, D. Rhodri Davies, Mitchell G. Mihalynuk

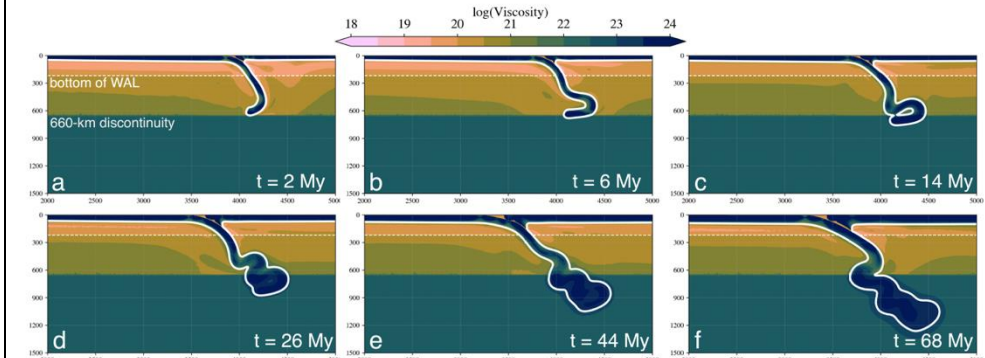
First published: 02 August 2022 | <https://doi.org/10.1029/2022JB024494> | Citations: 6

[Read the full text >](#)

 PDF  TOOLS  SHARE

Abstract

On Earth, the velocity at which subducting plates are consumed at their trenches (termed "subduction rate" herein) is typically 3 times higher than trench migration velocities. The subduction rate is also 5 times higher than estimated lower mantle slab sinking rates. Using simple kinematic analyses, we show that if this present-day "kinematic state" operated into the past, the subducting lithosphere should have accumulated and folded beneath near-stationary trenches. These predictions are consistent with seismic



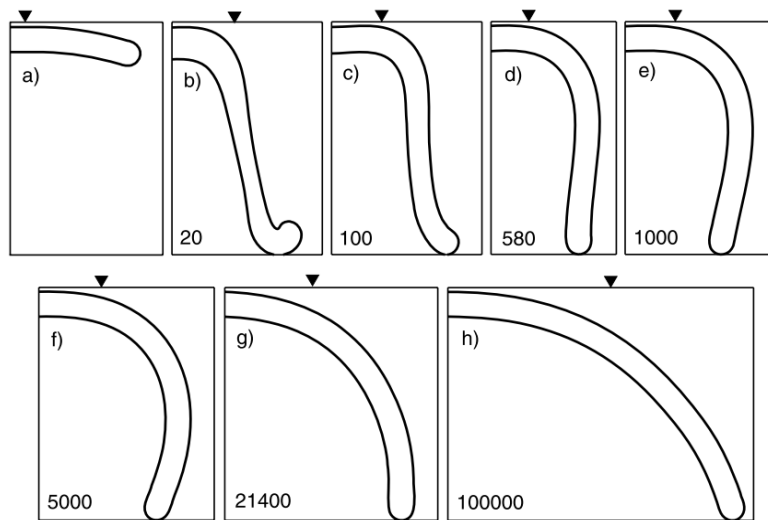
(deep slab) Mantle rheology and subduction dynamics

(deep slab) Mantle rheology and subduction dynamics

Various lines of evidence for relatively *weak slabs*.

- Slab shapes/trench motions: $\eta' = 100-500^*$
- Geoid: $\eta' \sim 10-100^{\#}$
- Plate bending considerations: $\eta' = 50-300^{\$}$

*Stegman et al., 2006; Ribe, 2010; Funiciello et al., 2008; Petersen et al., 2016; [#]Mao and Zhong, 2020; Moresi and Gurnis, 1996; ^{\$}Conrad and Hager, 1999; Wu et al., 2008.



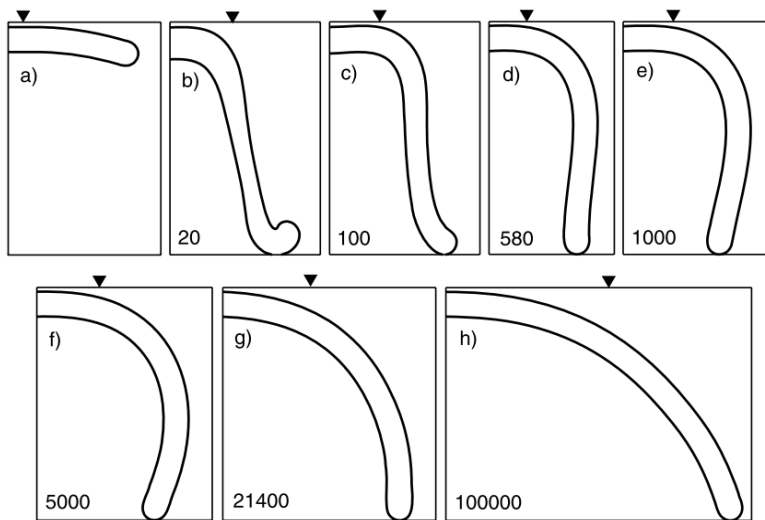
Ribe, 2010

(deep slab) Mantle rheology and subduction dynamics

Various lines of evidence for reduced viscosity slabs

- Slab shapes/trench motion
- Geoid:
- Plate bending considerations

*Stegman et al., 2006; Ribe, 2010; Funiciello et al., 2008; P. Zhong, 2020; Moresi and Gurnis, 1996; \$Conrad and Hager,



Ribe, 2010

Geochemistry, Geophysics, Geosystems®

Free Access

Subducting slabs: Jellyfishes in the Earth's mantle

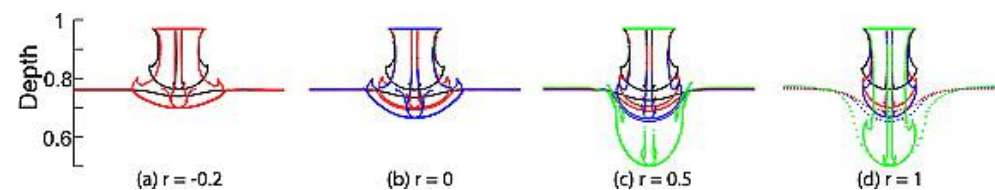
Christelle Loiselet , Jean Braun , Laurent Husson , Christian Le Carlier de Veslud , Cedric Thieulot , Philippe Yamato , Djordje Grujic

First published: 20 August 2010 | <https://doi.org/10.1029/2010GC003172> | Citations: 24

SECTIONS **SHARE**

Abstract

[1] The constantly improving resolution of geophysical data, seismic tomography and seismicity in particular, shows that the lithosphere does not subduct as a slab of uniform thickness but is rather thinned in the upper mantle and thickened around the transition zone between the upper and lower mantle. This observation has traditionally been interpreted as evidence for the buckling and piling of slabs at the boundary between the upper and lower mantle, where a strong contrast in viscosity may exist and cause resistance to the penetration of slabs into the lower mantle. The distribution and character of seismicity reveal, however, that slabs undergo vertical extension in the upper mantle and compression near the transition zone. In this paper, we demonstrate that during the subduction process, the shape of low viscosity slabs (1 to 100 times more viscous than the surrounding mantle) evolves toward an inverted plume shape that we coin *jellyfish*. Results of a 3D numerical model show that the leading tip of slabs deform



(deep slab) Mantle rheology and subduction dynamics

Various lines of evidence for relatively *weak slabs*.

- Slab shapes/trench motions: $\eta' = 100\text{-}500^*$
- Geoid: $\eta' \sim 10\text{-}100^\#$
- Plate bending considerations: $\eta' = 50\text{-}300^\$$

*Stegman et al., 2006; Ribe, 2010; Funiciello et al., 2008; Petersen et al., 2016; #Mao and Zhong, 2020; Moresi and Gurnis, 1996; \$Conrad and Hager, 1999; Wu et al., 2008.

Rheologic controls on slab dynamics

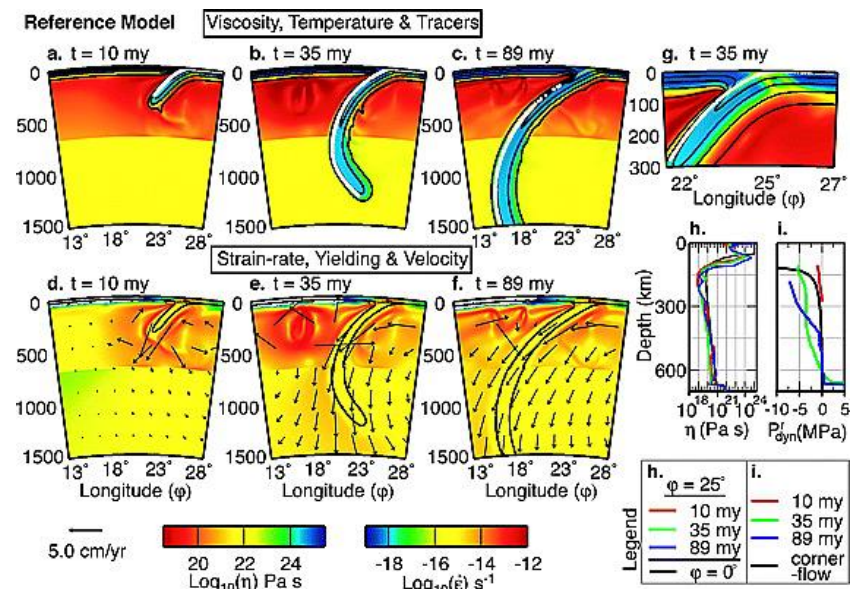
Magali I. Billen

Department of Geology, University of California Davis, One Shields Avenue, Davis, California 95616, USA
billen@geology.ucdavis.edu

Greg Hirth

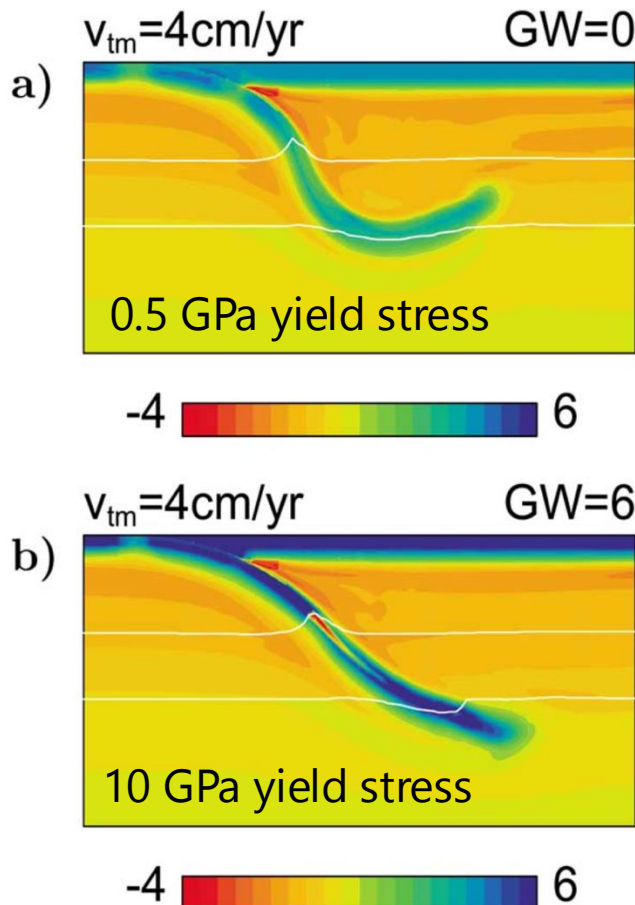
Department of Geology and Geophysics, Woods Hole Oceanographic Institution, Woods Hole, Massachusetts 02543, USA
girth@whoi.edu

[1] Several models have been proposed to relate slab geometry to parameters such as plate velocity or plate age. However, studies on the observed relationships between slab geometry and a wide range of subduction parameters show that there is not a simple global relationship between slab geometry and any one of these other subduction parameters for all subduction zones. Numerical and laboratory models of subduction provide a method to explore the relative importance of different physical processes in determining subduction dynamics. Employing 2-D numerical models with a viscosity structure constrained by laboratory experiments for the deformation of olivine, we show that the observed range in slab dip and the observed trends between slab dip and convergence velocity, subducting plate age, and subduction duration can be reproduced without trench motion (i.e., slab roll-back) for locations away from slab edges. Successful models include a stiff slab that is 100–1000 times more viscous than previous estimates from models of plate bending, the geoid, and global plate motions. We find that slab dip in the upper mantle depends primarily on slab strength and plate boundary coupling, with a small dependence on subducting plate age. Once the slab sinks into the lower mantle the primary processes controlling slab evolution are (1) the ability of the stiff slab to transmit stresses up dip, (2) resistance to slab descent into the higher-viscosity lower mantle, and (3) subduction-induced flow in the mantle-wedge corner.



But a few studies do argue for somewhat stronger slabs

(deep slab) Mantle rheology and subduction dynamics

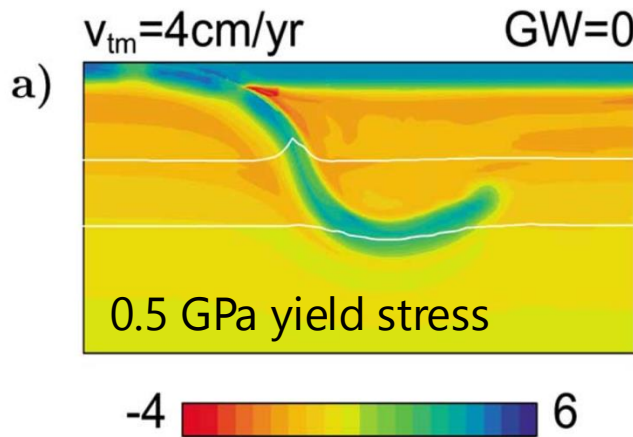


Cizkova et al. (2002)

Early study exploring the impact of slab weakening (grain size reduction in the cold slab interior, low-T plasticity) and trench motion on deep slab morphology.

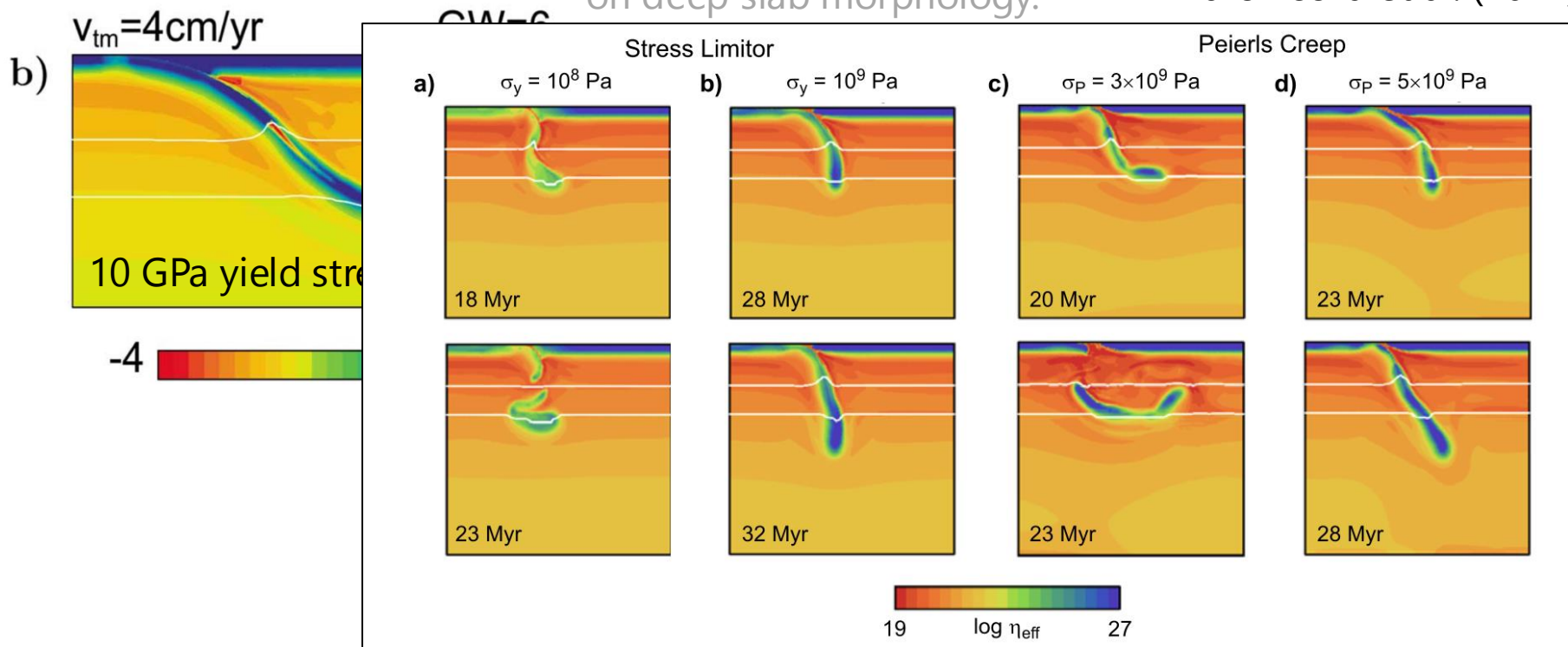
*Stegman et al., 2006; Ribe, 2010; Funiciello et al., 2008; Petersen et al., 2016; #Mao and Zhong, 2020; Moresi and Gurnis, 1996; \$Conrad and Hager, 1999; Wu et al., 2008.

(deep slab) Mantle rheology and subduction dynamics



Cizkova et al. (2002)

Early study exploring the impact of slab weakening (grain size reduction in the cold slab interior, low-T plasticity) and trench motion on deep slab morphology.



Androvicova et al. (2012)

(deep slab) Mantle rheology and subduction dynamics

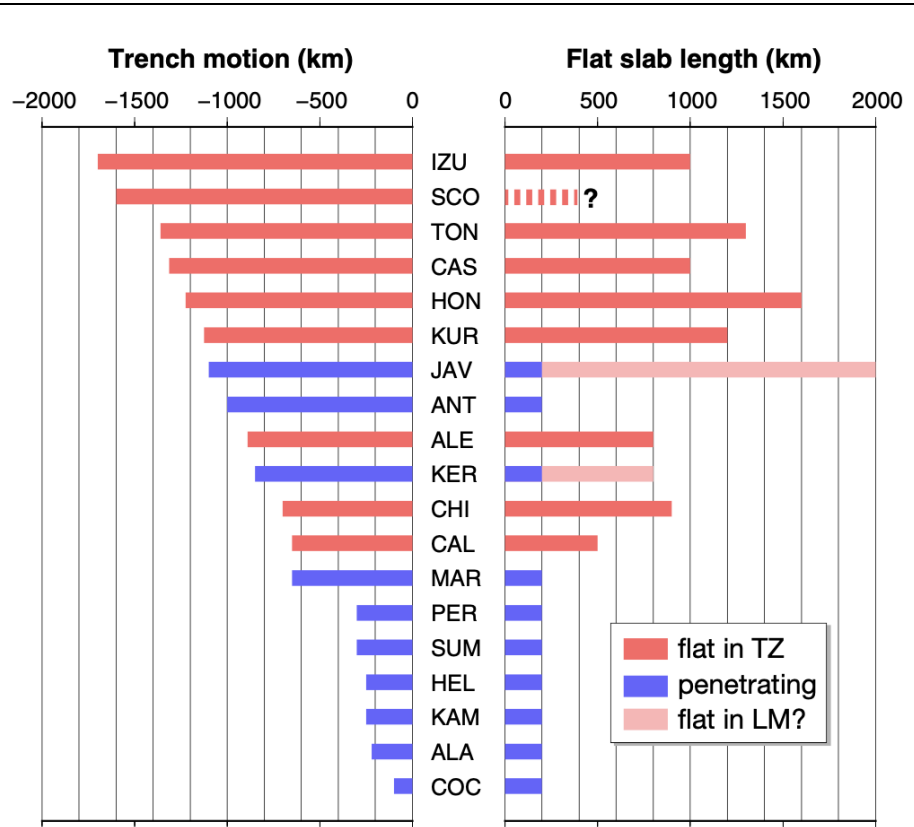
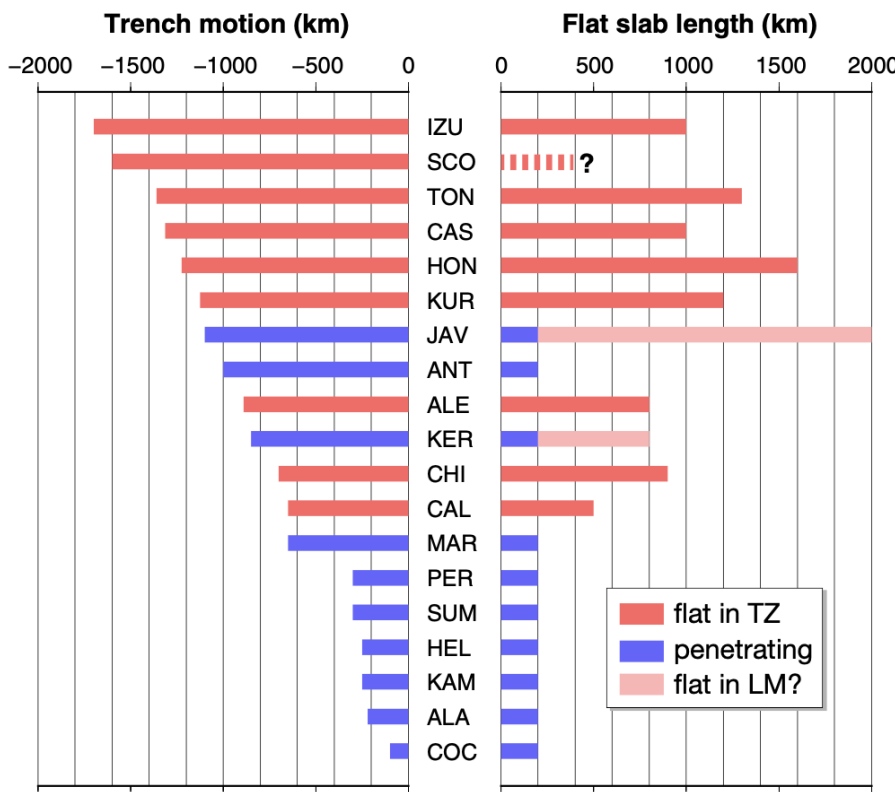


Figure 4. Estimates of total trench retreat over the past ~50 m.y. compared with the estimates of flat-slab length from Figure 2. Distances of trench retreat approximately perpendicular to the trench have been compiled from Ross and Scotese (1988), Jolivet and Faccenna (2000), Barker (2001), Faccenna et al. (2001), Schellart et al. (2003), Replumaz et al. (2004), Miller et al. (2006), Sdrolias and Müller (2006), Ren et al. (2007), Müller et al. (2008), and Schellart and Spakman (2012). For penetrating slabs, a thickness of 200 km is assigned because all of them thicken as they enter the lower mantle (LM). For the Scotia flat slab, no length can be estimated. Bright red bars are for slabs that flatten in the transition zone (TZ); light red bars for those that have been proposed to flatten below 700 km depth. Blue bars are for slabs that penetrate into the lower mantle. Flat-slab lengths and abbreviations as in Figure 2.

But trench motion proposal the greatest control on deep slab morphology (Goes et al., 2017)

(deep slab) Mantle rheology and subduction dynamics



As shown in models a long time ago
(Christensen, 1996)

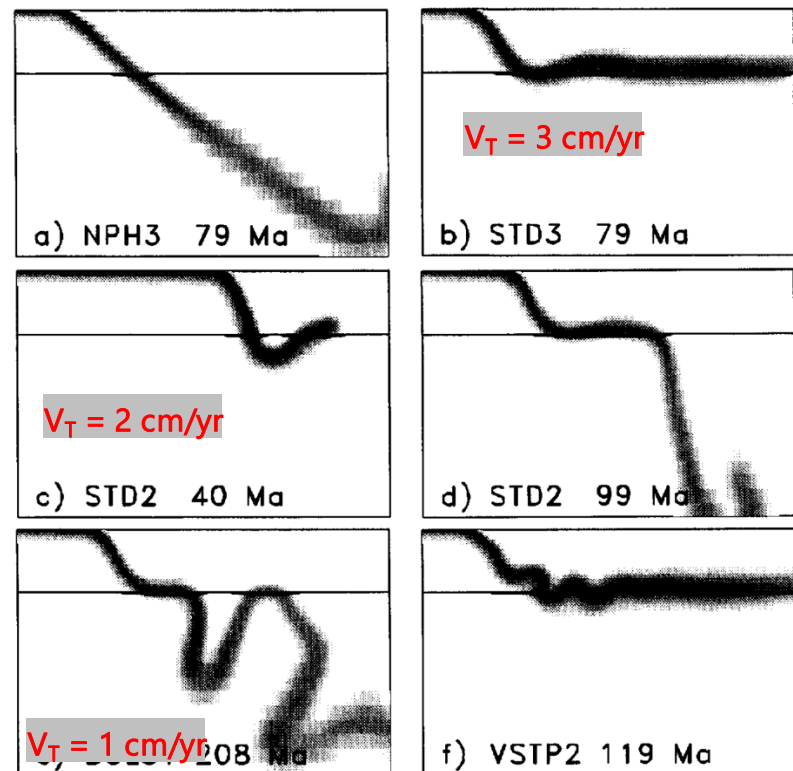


Figure 4. Estimates of total trench retreat over the past ~50 m.y. compared with the estimates of flat-slab length from Figure 2. Distances of trench retreat approximately perpendicular to the trench have been compiled from Ross and Scotese (1988), Jolivet and Faccenna (2000), Barker (2001), Faccenna et al. (2001), Schellart et al. (2003), Replumaz et al. (2004), Miller et al. (2006), Sdrolias and Müller (2006), Ren et al. (2007), Müller et al. (2008), and Schellart and Spakman (2012). For penetrating slabs, a thickness of 200 km is assigned because all of them thicken as they enter the lower mantle (LM). For the Scotia flat slab, no length can be estimated. Bright red bars are for slabs that flatten in the transition zone (TZ); light red bars for those that have been proposed to flatten below 700 km depth. Blue bars are for slabs that penetrate into the lower mantle. Flat-slab lengths and abbreviations as in Figure 2.

But trench motion proposal the greatest control on deep slab morphology (Goes et al., 2017)

(deep slab) Mantle rheology and subduction dynamics

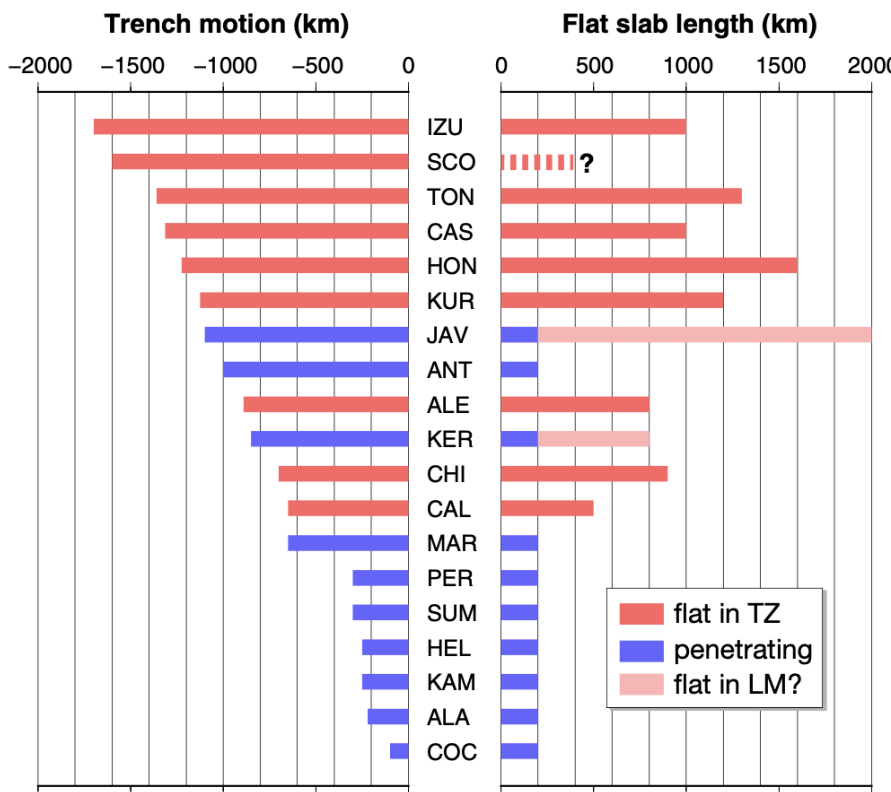
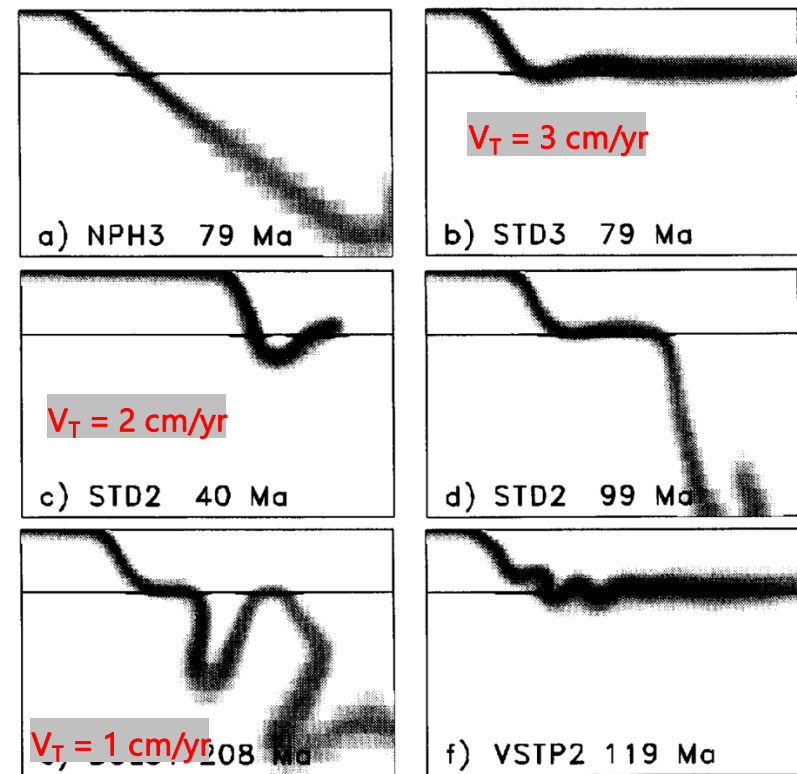


Figure 4. Estimates of total trench retreat over the past ~50 m.y. compared with the estimates of flat-slab length from Figure 2. Distances of trench retreat approximately perpendicular to the trench have been compiled from Ross and Scotese (1988), Jolivet and Faccenna (2000), Barker (2001), Faccenna et al. (2001), Schellart et al. (2003), Replumaz et al. (2004), Miller et al. (2006), Sdrolias and Müller (2006), Ren et al. (2007), Müller et al. (2008), and Schellart and Spakman (2012). For penetrating slabs, a thickness of 200 km is assigned because all of them thicken as they enter the lower mantle (LM). For the Scotia flat slab, no length can be estimated. Bright red bars are for slabs that flatten in the transition zone (TZ); light red bars for those that have been proposed to flatten below 700 km depth. Blue bars are for slabs that penetrate into the lower mantle. Flat-slab lengths and abbreviations as in Figure 2.

As shown in models a long time ago
(Christensen, 1996)

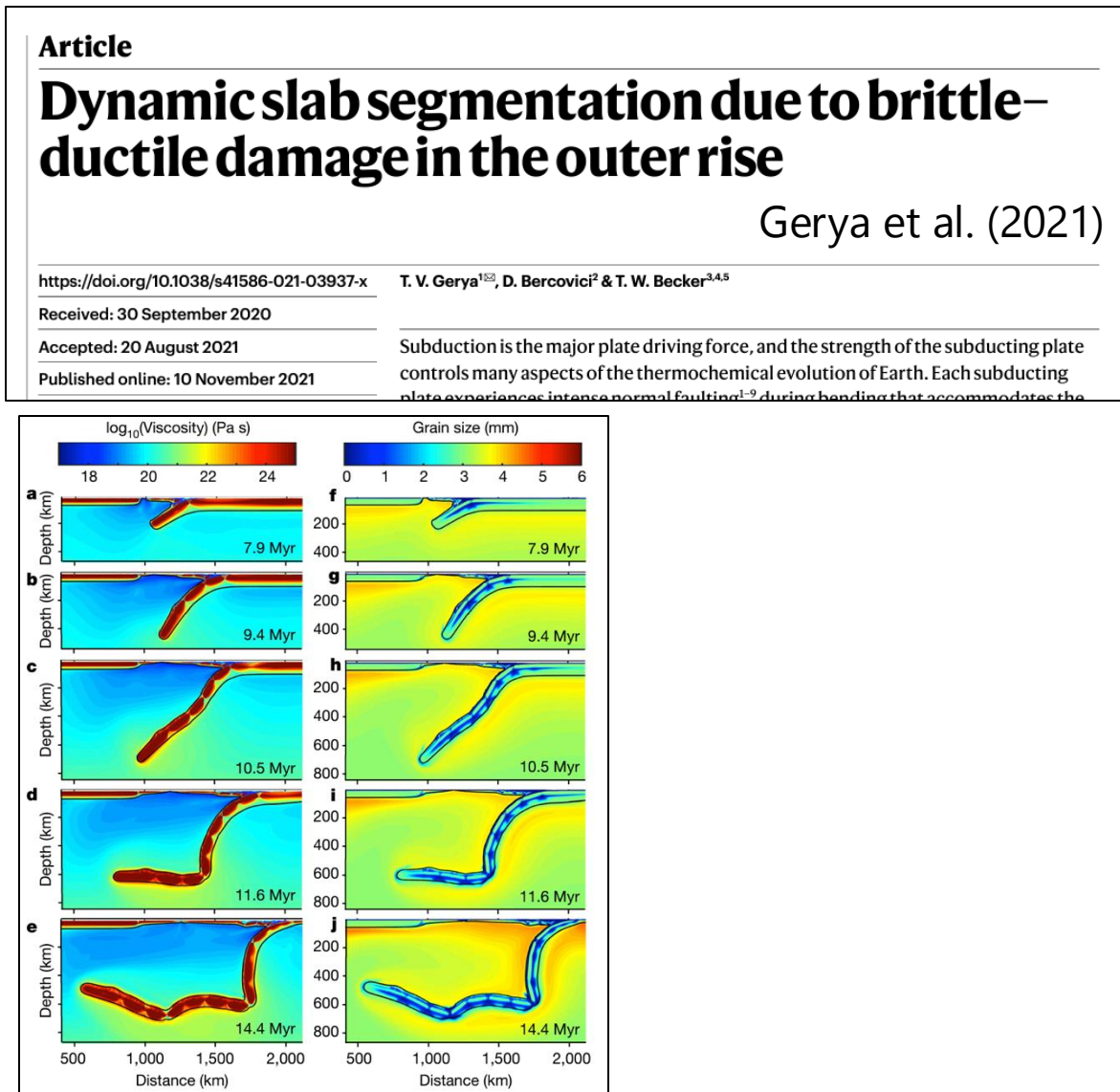


Phase transitions and how the lower mantle is also extremely important!
(e.g., Agrusta et al., 2014; 2017)

But trench motion proposal the greatest control on deep slab morphology (Goes et al., 2017)

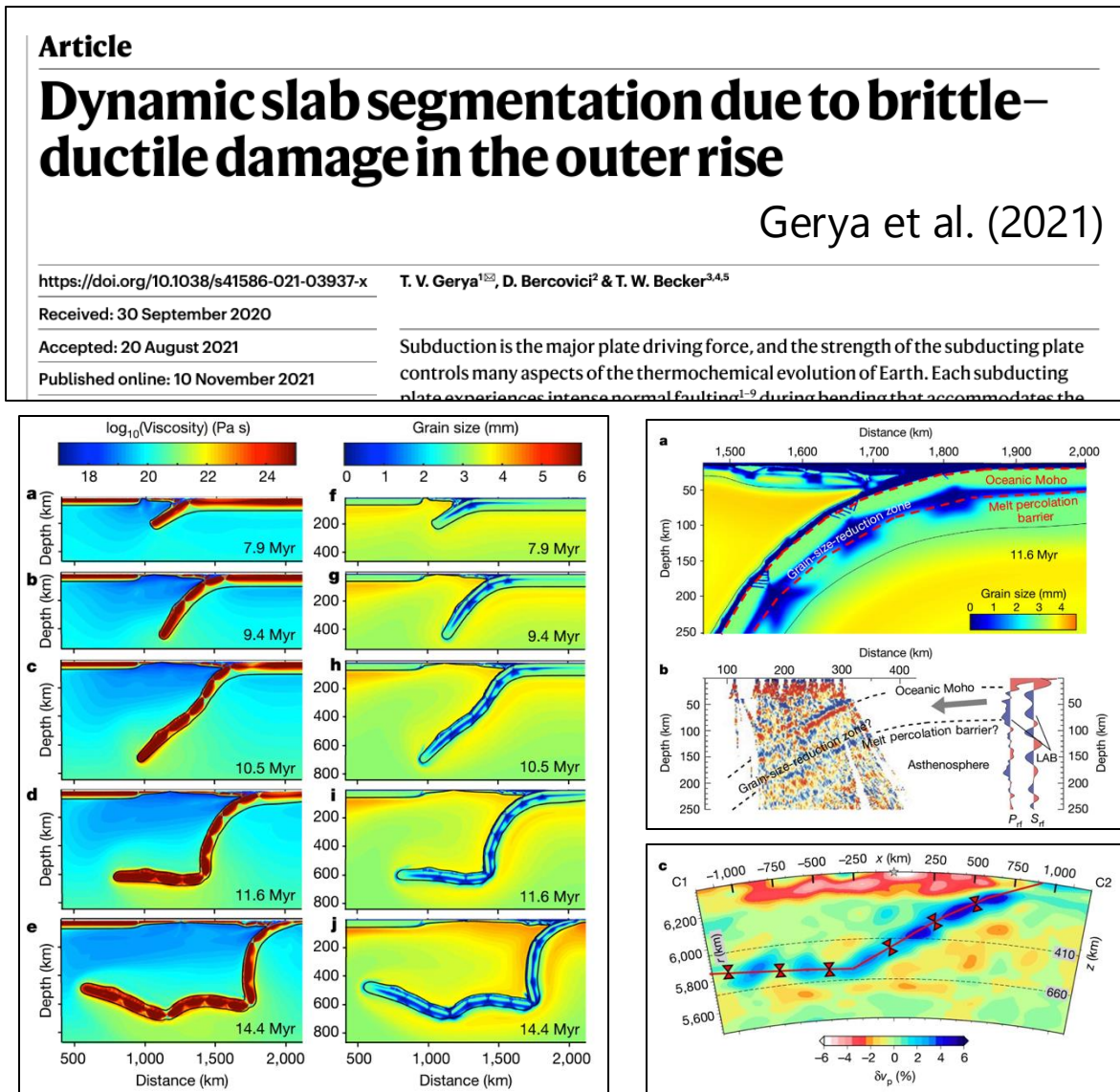
(deep slab) Mantle rheology and subduction dynamics

More complex slab rheologies (e.g., with “damage” inherited from brittle yielding in the outer wise) natural produce more complex slab shapes.

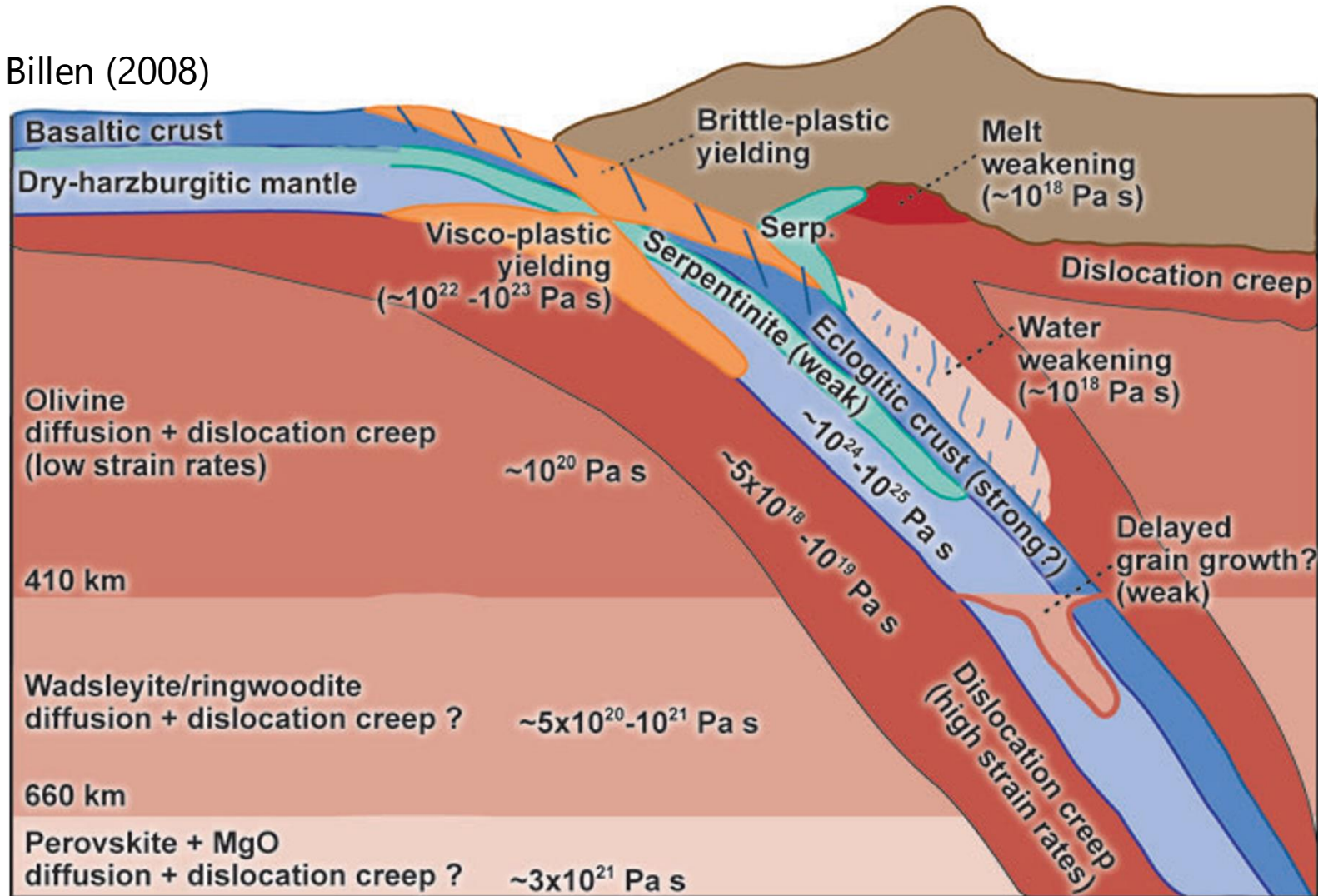


(deep slab) Mantle rheology and subduction dynamics

More complex slab rheologies (e.g., with “damage” inherited from brittle yielding in the outer rise) naturally produce more complex slab shapes.



Billen (2008)



Of course, most of these studies are missing plenty of additional details...

Stress and deformation mechanisms at a subduction zone: insights from 2-D thermomechanical numerical modelling

Annelore Bessat¹, Thibault Duretz,^{2,1} György Hetényi¹, Sébastien Pilet¹ and Stefan M. Schmalholz¹

¹*Institute of Earth Sciences, University of Lausanne, 1015 Lausanne, Switzerland. E-mail: annelore.bessat@unil.ch*

²*Univ Rennes, CNRS, Géosciences Rennes – UMR 6118, F-35000 Rennes, France*

Accepted 2020 February 17. Received 2020 January 30; in original form 2019 July 14

SUMMARY

Numerous processes such as metamorphic reactions, fluid and melt transfer and earthquakes occur at a subducting zone, but are still incompletely understood. These processes are affected, or even controlled, by the magnitude and distribution of stress and deformation mechanism. To eventually understand subduction zone processes, we quantify here stresses and deformation mechanisms in and around a subducting lithosphere, surrounded by asthenosphere and overlain by an overriding plate. We use 2-D thermomechanical numerical simulations based on the finite difference and marker-in-cell method and consider a 3200 km wide and 660 km deep numerical domain with a resolution of 1 km by 1 km. We apply a combined visco-elasto-plastic deformation behaviour using a linear combination of diffusion creep, dislocation creep and Peierls creep for the viscous deformation. We consider two end-member subduction scenarios: